Chem Soc Rev

Single-crystal polymers (SCPs): from 1D to 3D architectures

Journal:	*Chemical Society Reviews*
Manuscript ID	CS-REV-07-2023-000553.R2
Article Type:	Review Article
Date Submitted by the Author:	01-Oct-2023
Complete List of Authors:	Wang, Mingsen; Qingdao University of Science and Technology, College of Polymer Science and Engineering Jin, Yinghua; University of Colorado Boulder, Chemistry Zhang, Wei; University of Colorado Boulder, Department of Chemistry Zhao, Yingjie; Qingdao University of Science and Technology, College of Polymer Science and Engineering

ARTICLE

Single-crystal polymers (SCPs): from 1D to 3D architectures

Mingsen Wang,[a] Yinghua Jin,[b] Wei Zhang,*[b] and Yingjie Zhao*[a]

Received 00th January 20xx,
Accepted 00th January 20xx

DOI: 10.1039/x0xx00000x

Single-crystal polymers (SCPs) with unambiguous chemical structures at atomic-level resolutions have attracted great attention. Obtaining precise structural information of these materials is critical as it enables a deeper understanding of the potential driving forces for specific packing and long-range order, secondary interactions, kinetic and thermodynamic factors. Such information can ultimately lead to success in controlling the synthesis or engineering of their crystal structures for targeted applications, which could have far-reaching impact. The successful synthesis of SCPs with an atomic level control of the structures, especially for those with 2D and 3D architectures, has been rare. In this review, we summarize the recent progress in the synthesis of SCPs, including 1D, 2D, and 3D architectures. Solution synthesis, topochemical synthesis, and extreme condition synthesis were summarized and compared. Around 70 examples of SCPs with unambiguous structure information were presented, and their synthesis methods and structural analysis were discussed. This review offers critical insights into the structure-property relationships, providing guidance for the future rational design and bottom-up synthesis of a variety of highly ordered polymers with unprecedented functions and properties.

Introduction

Since Staudinger proposed the definition of macromolecule in the early 1920s,[1, 2] traditional linear polymers (one-dimensional (1D) polymers) have been studied extensively within the past century. In 2004, The successful exfoliation of the graphene monolayer from graphite expanded the structure of the traditional linear (1D) polymers to two-dimensional (2D) networks,[3] ushering in "2D" era. In 2005, Yaghi and co-workers synthesized the first example of 2D covalent organic frameworks (COFs) through a facile solution synthesis.[4] Subsequently, the first example of 3D COFs was reported by the Yaghi group in 2007.[5] Since then, diversified polymeric structures with complex 2D and 3D topologies have been achieved through deliberate control and manipulation of the building blocks and synthetic conditions.[6, 7] Despite the great advances in this field, there is still no straightforward way for preparing large single crystals of these 2D and 3D polymeric architectures with complete structural control, analogous to how nature creates 2D graphite or 3D diamond. Usually, polycrystalline powders are obtained through the kinetic polymerization process under solvothermal conditions.[8] The precise control of the polymerization in 2D or 3D spaces to obtain large-sized 2D or 3D single-crystal polymers (SCPs) has been a very challenging task. In 2014, the first example of a large-sized 2D SCPs was successfully prepared by Schlüter and co-workers through topochemical polymerization.[9] The breakthrough of the synthesis of a large-sized single-crystal 3D COFs from solution was realized by Wuest, Wang, and Yaghi.[10, 11] The single-crystal polymeric structures with atomic resolution is critical in understanding many fundamental questions. For example, how can we achieve long-range order through the packing and secondary interactions of 1D polymer chains? What are the exact stacking modes of the layers in 2D COFs along the c-axis direction? What are the exact interpenetrations in 3D COFs that are usually hard for the common powder X-ray diffraction (PXRD) to determine?[6, 8, 12-14] What is the arrangement of the guest molecules within the framework?[11] etc. There are still many unknowns in polymeric architectures, which has strongly impeded their structure-property relationship study, mechanism understanding, the exploration of structure-oriented applications, and the development of next-generation functional materials.

In this review, we summarize the recent development in the controlled synthesis of SCPs. We focus on the single crystals of 1D, 2D and 3D covalently linked polymers. The chosen examples of the SCPs discussed here should have unambiguous structures determined by either single-crystal X-ray diffraction (SCXRD) or electron diffraction technique,[14-16] which could give clear atomic-level structure information. The examples of SCPs are classified into 1D, 2D, and 3D architectures, which were further categorized based on the different synthetic strategies into solution synthesis, topochemical synthesis, and others (Fig. 1). Finally, the review concludes with perspectives on the current problems, possible solutions, and future endeavors, providing valuable perspectives on the field of SCPs.

[a] College of Polymer Science and Engineering, Qingdao University of Science and Technology, Qingdao 266000, China
[b] Department of Chemistry, University of Colorado Boulder, Boulder, Colorado 80309, United States

† Footnotes relating to the title and/or authors should appear here.
Electronic Supplementary Information (ESI) available: [details of any supplementary information available should be included here]. See DOI: 10.1039/x0xx00000x

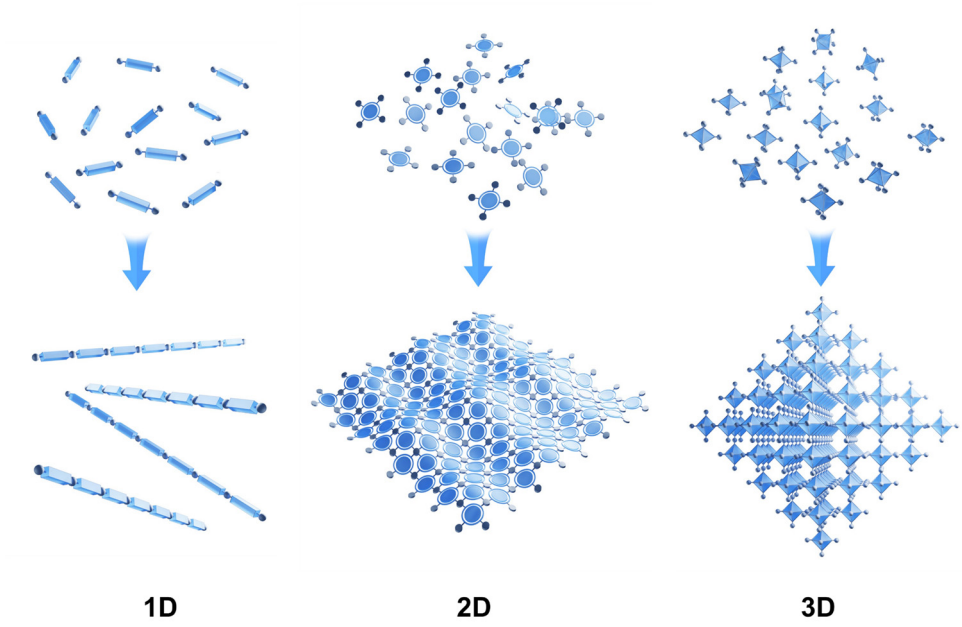

Fig. 1 Schematic diagram of the preparation of 1D, 2D and 3D architectures.

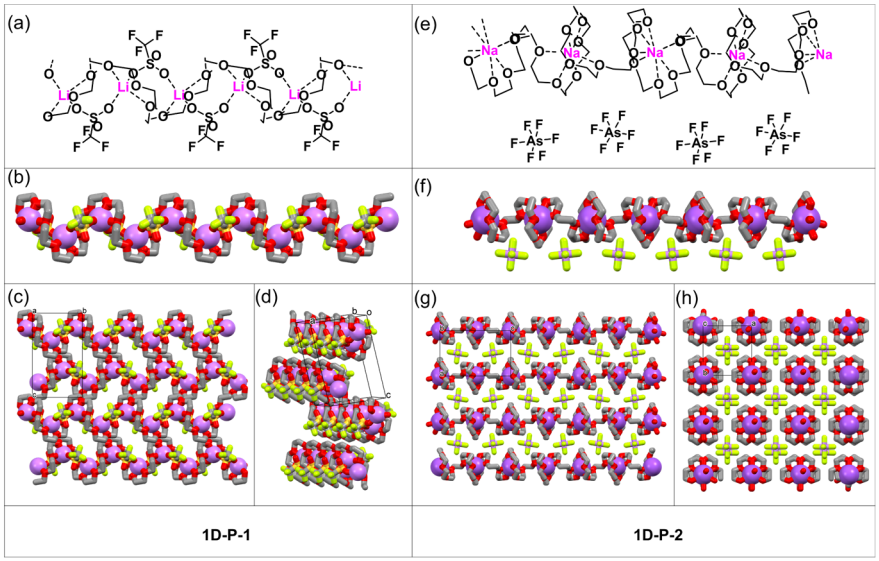

Fig. 2 1D polymer with metal-ligand interactions: (a) The chemical structure of **1D-P-1**. (b) The single-crystal structure of a single-chain of **1D-P-1**. (c) View of the packing mode along the *a*-axis. (d) View of the packing mode along the *b*-axis. (e) The chemical structure of **1D-P-2**. (f) The single-crystal structure of a single-chain of **1D-P-2**. (g) View of the packing mode along the *b*-axis. (h) View of the packing mode along the *c*-axis.

1. 1D Architectures

1.1 Recrystallization

1D polymers, also known as linear polymers, have been a topic of research for more than 100 years. Due to the good solubility of most 1D polymers, the growth of the single crystals could be realized by the recrystallization process similar to the case of small molecules.[17-20] Even so, compared to small molecules, the reported single crystals of 1D polymers with unambiguous atom-level structure information are still rare.[21-25] Significant research efforts have been devoted to the controlled synthesis of 1D SCPs.[26-29]

High-quality single crystals of 1D polymer are not easily available or accessible because high molecular weight 1D polymers often form powders or spherulitic films when they are crystalline. In 2003, Henderson and co-workers successfully obtained a single crystal of **1D-P-1** from a low molecular weight polyethylene oxide (PEO) (Fig. 2a).[30] The solution of 1D polymer $P(EO)_3(500)$ and $LiCF_3SO_3$ mixture was kept in a dry room for several weeks to give long needle-like single crystals. The single crystal **1D-P-1** was analyzed by SCXRD, which revealed a monoclinic unit cell with space group $P2_1/n$. It should be noted that each Li^+ cation is coordinated with three oxygen atoms from PEO and two oxygen donors from two $CF_3SO_3^-$ anions (Fig. 2b). A linear helical chain was formed using the Li^+ cation as a

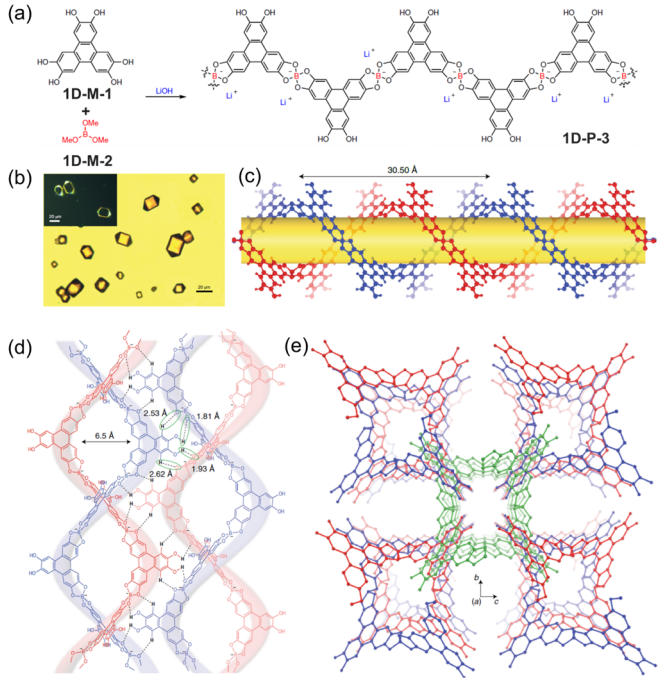

Fig. 3 Helical 1D polymer with hydrogen bonding: (a) Synthesis of the 1D helical polymer **1D-P-3**; (b) Optical images of the large single crystals of **1D-P-3**; (c) A stick representation of the strands along the *b*-axis; (d) Formation of helical strands through hydrogen-bonding interactions along the *a* axis; (e) The view along the *a*-axis. Reproduced with permission from ref. 58, Copyright 2021, Springer Nature.

template. These linear chains are stacked in parallel to form single crystals (Fig. 2c, d).

Bruce and co-workers reported a **1D-P-2** single crystal with sufficient quality for SCXRD (Fig. 2e).[31] The single crystal was grown by combining $NaAsF_6$ salt with PEO in acetonitrile, followed by slow evaporation. Experimental and simulated PXRD patterns show excellent agreement, indicating the bulk powder sample has the same crystalline phase as the single crystal. Similar to the structure of **1D-P-1**, the SCXRD reveals that Li^+ cations are coordinated with the oxygen atoms in the polymer chain, leading to the formation of a helical structure (Fig. 2f, g, h).

1.2 Solution Synthesis

While the crystallization of 1D polymer solutions can lead to the formation of SCPs in a relatively easy way, the strategy is highly dependent on the solubility and the molecular weight of the polymers. As a result, there has been a growing interest in direct synthetic strategies of SCPs in solution. The development of dynamic covalent chemistry has contributed significantly to constructing highly ordered structures, such as COFs, through solution synthesis.[32-43] The self-correction process in dynamic covalent chemistry enables the formation of SCPs with high degrees of structural order.[44-55] Compared to 2D and 3D COFs, the synthesis of lower dimensional 1D COFs in solution has been less reported. The 1D COFs synthesis is hampered by the anisotropy and the entropy-driven random packing of the linear organic chains.[56] The high symmetries and limited freedom of the intermolecular packing in 2D or 3D COFs usually facilitate their crystallization process. In 1D COFs, the molecular packing is more flexible because their covalent links are confined to a single dimension. [56, 57] Therefore, external noncovalent interactions, such as hydrogen bonding, hydrophobic interactions, or π-π stacking interactions, are generally needed to form ordered crystalline structures of 1D COFs.

Zhang and co-workers recently reported a 1D helical SCP.[58] The single-crystalline helical structures through either the hydrogen bond or metal coordination have been reported by Huc, Nitschke, etc.[59-62] In this work, the 1D polymer **1D-P-3** was synthesized through a condensation reaction of **1D-M-1** with **1D-M-2** in the presence of LiOH (Fig. 3a). Large-sized single crystals were formed during the polymerization in a solution (Fig. 3b). Based on the assumption that all three diol groups would be converted into spiroborate linkages, a 2D COF was expected to form by consuming the **1D-M-1** and **1D-M-2** at a ratio of 2:3. Unexpectedly, only two pairs of diols in each **1D-M-1** participated in the reaction, forming 1D zigzag-shaped polymer chains (Fig. 3a, c). The hydrogen bond interactions between the spiroborate units and the unreacted diols provide the energy gain and stabilization, which led to the formation of the unusual helical backbone (Fig. 3d). Notably, the helical strands form double helices not through strong noncovalent interactions between the two strands of the same pair but through the hydrogen bonding interactions with the strand of a neighboring helical pair (mechanically entwined) (Fig. 3e). This is very different from DNA and most of the reported synthetic double-helical polymers in which the pair of strands are usually packed together through the noncovalent interactions within the pair.

In addition to hydrogen bonding interactions, metal-ligand interactions have also been found critical in forming 1D SCP structures with structural order. Loh and co-workers combined the reversibility of metal coordination bonds and dynamic covalent bonds to prepare the 1D covalent SCPs (**1D-P-4**).[56] As shown in Fig. 4a, the polymerization of the two monomers **1D-M-3** and **1D-M-4** led to the poorly crystalline 1D conjugated polymer. Notably, when a suitable amount of $AgBF_4$ was introduced, self-assembly of the linear polymer chains via coordination occurred, yielding micrometer-sized 1D metallo-COF single crystals (**1D-P-4**) (Fig. 4b). Single-crystal electron diffraction (SCED) with a resolution of ~0.95 Å shows a zigzag packing mode (Fig. 4c). Moreover, further polymerization in the crystalline state led to the formation of a 3D woven network while preserving the original polymer backbone (Fig. 4d).

The same group subsequently reported a similar example in which copper ions were used instead of silver ions (Fig. 5a).[63] The polymerization of a homoleptic complex **1D-M-5** and a polydentate linker **1D-M-4** produced a heteroleptic species through ligand exchange, resulting in the formation of a 1D COF (**1D-P-5**) (Fig. 5a). The structure of the obtained **1D-P-5** was confirmed by PXRD and three-dimensional electron diffraction analysis (3D ED). In **1D-P-5**, **1D-M-3** molecules are arranged orderly along the conjugated zigzag backbones formed by imine-linked phenanthroline (Fig. 5b).

These studies have demonstrated that the combined use of metal coordination and dynamic covalent chemistry could broaden the scope of COF synthesis. Most importantly, the

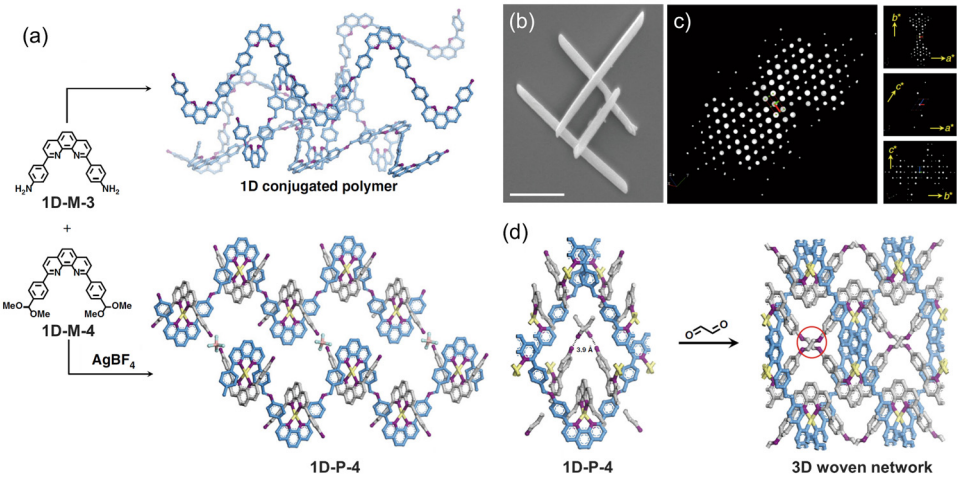

Fig. 4 Crystallization of a 1D COFs driven by metal-ligand coordination and their further formation of a 3D woven network: (a) Schematic illustration of 1D metallo-COF synthesis; (b) SEM image of **1D-P-4**; (c) The lattice of **1D-P-4** reconstructed from the SCED data; (d) Crystalline-state polymerization process. Reproduced with permission from ref. 56, Copyright 2020, Springer Nature.

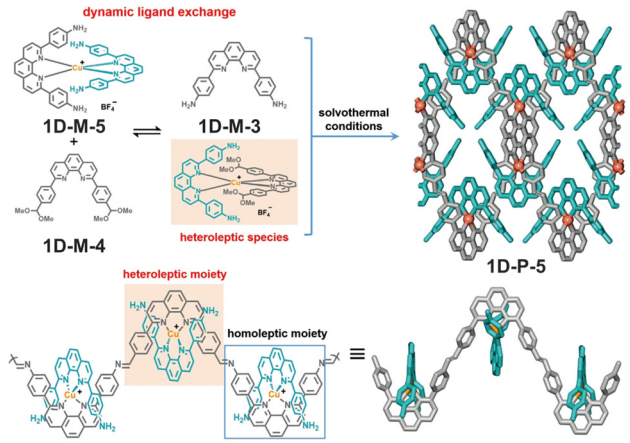

Fig. 5 Formation of 1D COF through dynamic ligand exchange: (a) Synthesis of **1D-P-5** and the chemical composition of a single zigzag chain; (b) Strategies for constructing **1D-P-5**. Reproduced with permission from ref. 63, Copyright 2020, Wiley-VCH.

introduction of metal coordination facilitates the growth of single crystals of 1D COFs. Besides 1D structures, this strategy has also been successfully used in the construction of 3D COFs single crystals. A detailed discussion of the 3D metal woven COFs will be presented in the later section of 3D architectures.

1.3 Topochemical polymerization

Topochemical reactions in a single-crystal state have been a hot subject of investigation for several decades.[64-68] The topochemical polymerization approach allows the preparation of SCPs from pre-assembled monomer crystals through a single-crystal-to-single-crystal (SCSC) transformation.[69-71] Compared to the solution-based synthesis, this solid-state synthesis provides a new method for preparing SCPs. However, this approach is highly dependent on the molecular packing within the single crystal of monomers. Although the strict geometric requirements of topochemical polymerizations and the challenges in monomer design have limited the generality of this approach, significant progress has been made. Various reaction types have been successfully employed, including [2 + 2],[72-77] [4 + 4],[9, 78-81] diene or triene polymerization,[82-84] quinodimethane polymerization,[85, 86] acetylenes polymerization[87-92] and azide-alkyne cycloaddition.[93-99] The examples of 1D SCPs obtained by SCSC transformation have also been reviewed in several excellent articles.[67, 70, 100-102]

1.3.1 [2+2] Photo-dimerization

The pioneering work of crystalline 1D polymers prepared in the solid state by the [2 + 2] photo-dimerization was reported in 1969 by Hasegawa and co-workers.[103] Since then, the [2 + 2] photo-dimerization has been widely utilized to synthesize 1D SCPs.[104-112] Recently, Stoddart and Guo employed the self-complementary effects of the pyridinium-based system due to their shape and charge distribution interactions and successfully prepared single-crystal polycationic polymers through [2+2] SCSC topochemical photopolymerization.[77] As shown in Fig. 6, a triolefinic tripyridinium monomer **1D-M-6** was first designed and synthesized, which adopts a conformation wherein two transstyrylpyridinium arms are oriented in one direction, while the third arm is oriented in the opposite direction. Two of three pyridinium arms adopt anti-parallel co-conformations with those in adjacent molecules to form an infinite linear superstructure in which all the neighboring monomers are integrated noncovalently in the crystal. The third arm of the monomer is free and does not form pairs with adjacent monomers. The subsequent irradiation of the monomer single crystals with ultraviolet light (λ = 365 nm) at 100 K for 9 hours resulted in the formation of 1D SCPs (**1D-P-6**). Subsequently, by using the same strategy, they successfully obtained another example of 1D SCP with very large molecular weights.[113] As shown in Fig. 7a, bipyridinium monomer **1D-M-7** was designed and synthesized, which can self-assemble into an infinite 1D supramolecular structure through anti-parallel co-conformations employing self-complementary interactions between pyridinium-based appendages. 1D SCP **1D-P-7** was obtained by irradiating the monomer crystals with UV light at 100 K for 6 hours. Notably, **1D-P-7** exhibits good solubility in

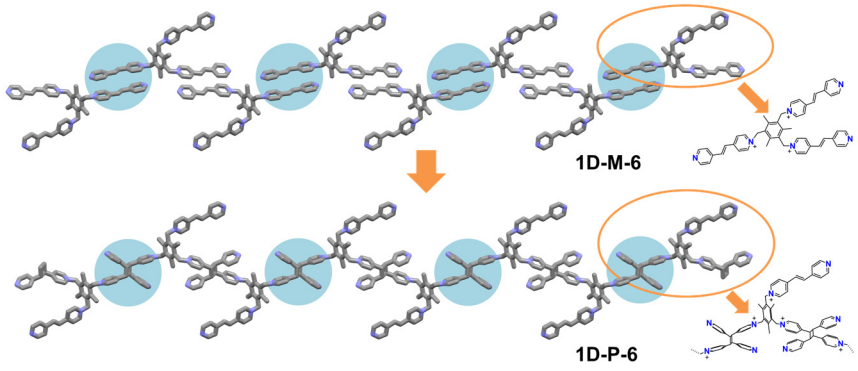

Fig. 6 The single-crystal X-ray structures of **1D-M-6** and **1D-P-6.**

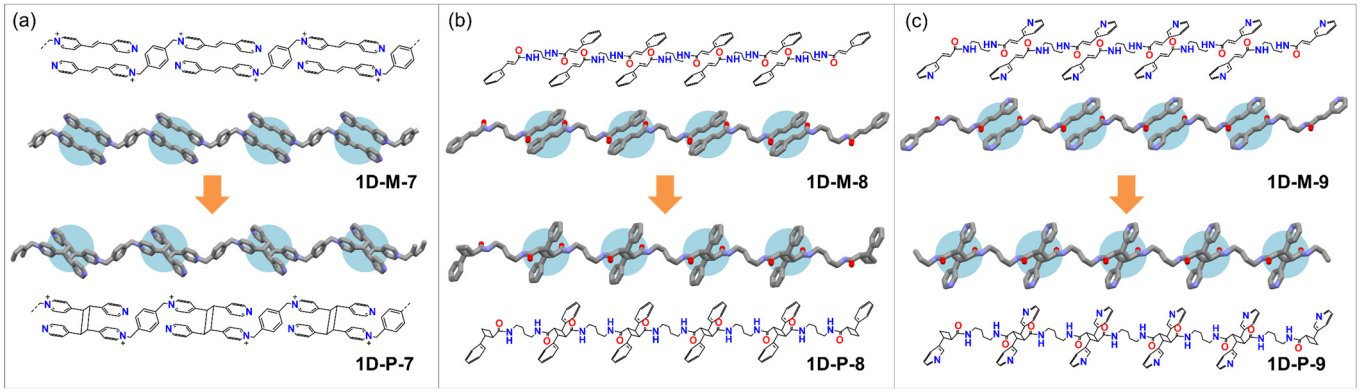

Fig. 7 The chemical and single-crystal X-ray structures of (a) **1D-M-7** and **1D-P-7**; (b) **1D-M-8** and **1D-P-8**; (c) **1D-M-9** and **1D-P-9.**

strong polar solvents, which enables their in-depth characterization in the solution phase.

Biradha and co-workers reported two examples of 1D SCPs through [2+2] photo-dimerization in single-crystal states.[75] As shown in Fig. 7b and c, **1D-M-8** and **1D-M-9** with similar structures were designed to contain bisamide groups. The potential hydrogen bond-induced secondary structures can promote the [2+2] photo-dimerization. **1D-M-8** and **1D-M-9** adopt 1D alignment of molecules along the *a*-axis arranged through π-π interactions between the amide and phenyl or pyridyl groups. Irradiation of the single crystals of **1D-M-8** and **1D-M-9** under sunlight for 22 hours results in the [2+2] reaction occurring in an SCSC manner to yield single crystals of the **1D-P-8** and **1D-P-9**. The strong hydrogen-bonding interactions of the bisamide groups induced 2D layered structures, which also promoted the [2+2] polymerization reaction.

1.3.2 [4 + 4] Photo-dimerization

Schlüter and Servalli reported a novel ladder-type 1D SCP example through the [4 + 4] photo-dimerization of the anthracene-based monomer.[79] A desymmetrized anthracene-based monomer **1D-M-10** was designed with methoxy substituents to break the symmetry (Fig. 8a). Each **1D-M-10** molecule has two anthracene units face-to-face stacking with the anthracene units of its neighbors, leading to potential 1D polymer chains upon photoreaction. The photopolymerization in the single-crystal state was realized by the 15 min irradiation under 465 nm UV light. Monomer single crystals **1D-M-10** smoothly convert into polymer single crystals **1D-P-10**. Zhang and co-workers reported an example of platinum-based 1D SCP through the [4+4] cycloaddition of anthracene in an SCSC fashion.[78] They employ a platinum coordination-driven self-assembly strategy to secure the appropriate head-to-tail alignment of anthracene moieties in monomer 1**D-M-11** (Fig. 8b). The coordination-driven force induces an appropriate alignment of the 1**D-M-11**. The anthracene blades in 1**D-M-11** are aligned in a head-to-tail manner with strong π-π stacking between the anthracenes. The subsequent irradiation of the 1**D-M-11** single crystals with white light at 265 K for 9 days resulted in the formation of **1D-P-11**. Taking advantage of the temperature-dependent slow depolymerization, this Pt-based 1D polymer showed potential as a sustained-release anticancer drug platform.

1.3.3 Polymerization of dienes and trienes

The polymerization of 1,3-diene derivatives can also realize the SCSC topochemical reaction.[82, 83, 114-123] Matsumoto and co-workers reported a 1,3-diene dicarboxylic acid monomer **1D-M-12** with a substitution of a chlorine atom in the aromatic hydrogen of the benzyl group (Fig. 9a).[82] The SCXRD revealed that the planar diene moieties are closely packed to form a columnar structure in the crystals. Both weak halogen-halogen and CH/π interactions are important for the self-assembly of **1D-M-12** in an appropriate mode. The photoirradiation was carried out using γ-ray radiation at room temperature, leading to the successful polymerization of **1D-M-12** in a single-crystal

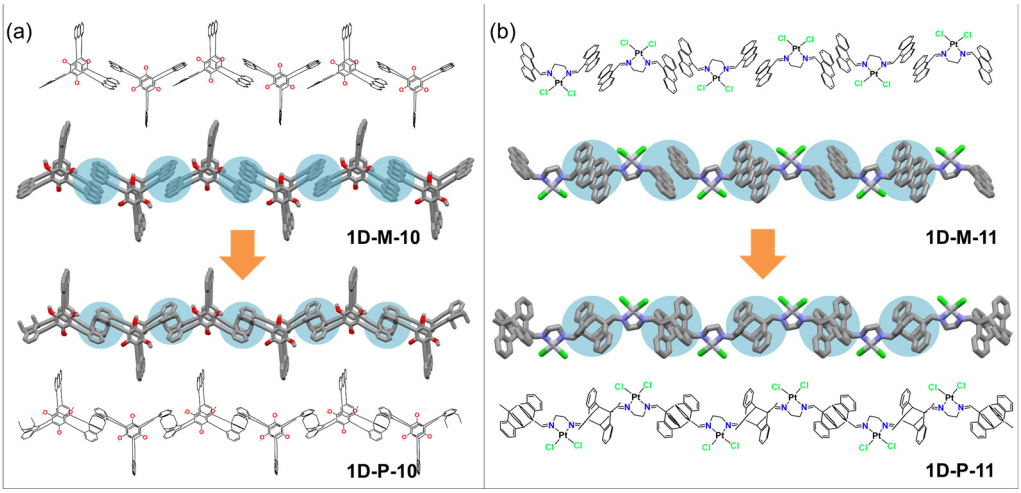

Fig. 8 The chemical and single-crystal X-ray structures of (a) **1D-M-10** and **1D-P-10**; (b) **1D-M-11** and **1D-P-11**.

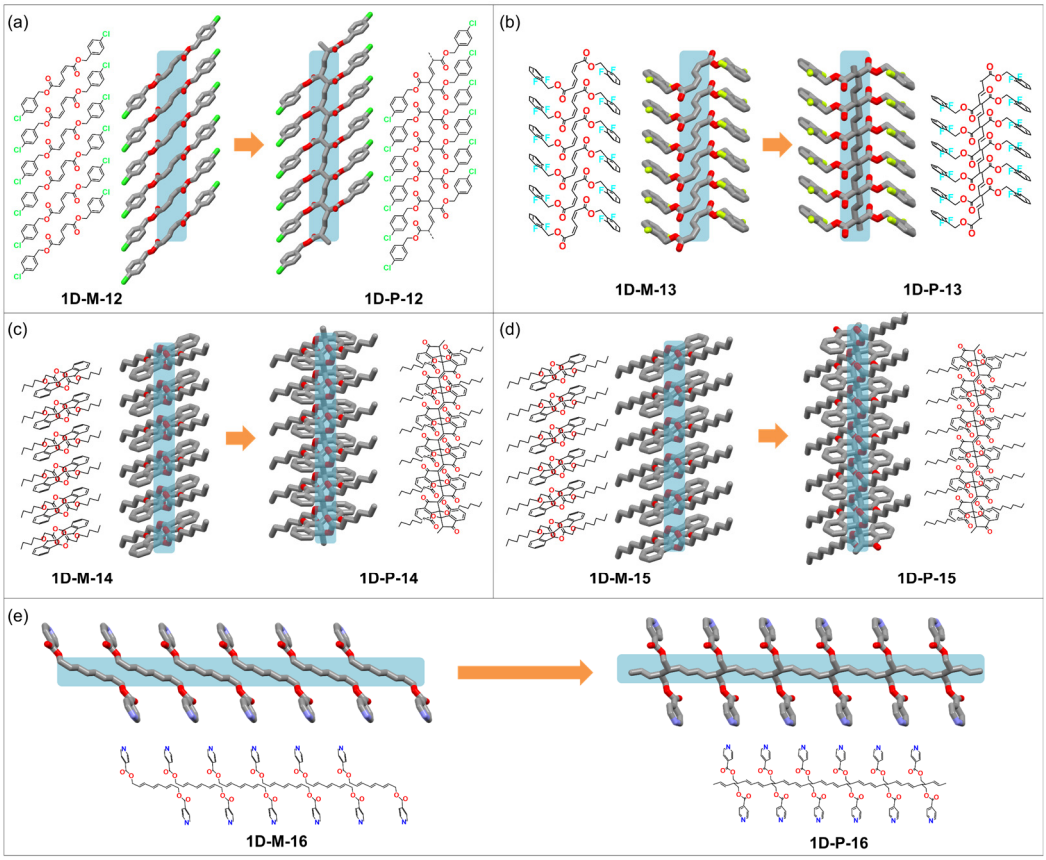

Fig. 9 The chemical and single-crystal X-ray structures of (a) **1D-M-12** and **1D-P-12**; (b) **1D-M-13** and **1D-P-13**; (c) **1D-M-14** and **1D-P-14**; (d) **1D-M-15** and **1D-P-15**; (e) **1D-M-16** and **1D-P-16**.

state. The topochemical polymerization of **1D-M-12** proceeds a transformation in the chemical bond with a minimum movement of atoms to produce 1D SCP **1D-P-12**. The same group further reported a fluorine-substituted **1D-M-13**, which has a similar structure to the chlorine-substituted **1D-M-12** (Fig. 9b).[124] The intermolecular interactions such as C-H…O and C-H…F interactions contribute to the formation of a columnar structure with appropriate molecular packing and thus realize the successful polymerization in the single-crystal state under γ-ray radiation to give 1D SCP **1D-P-13**. Interestingly, a dimer is exclusively produced under UV irradiation instead of polymerization. The columnar structure with an appropriate stacking distance is indispensable to the successful topochemical polymerization of such 1,3-diene monomers. The too large or small distance is unfavorable for the topochemical polymerization in a single crystal state.[125]

Wudl and co-workers realized the visible light-triggered topochemical polymerization reaction of two bi-indene-dione derivatives (**1D-M-14 and 1D-M-15**) in a single crystal state under sunlight or a high-pressure sodium lamp (Fig. 9c and d).[126]

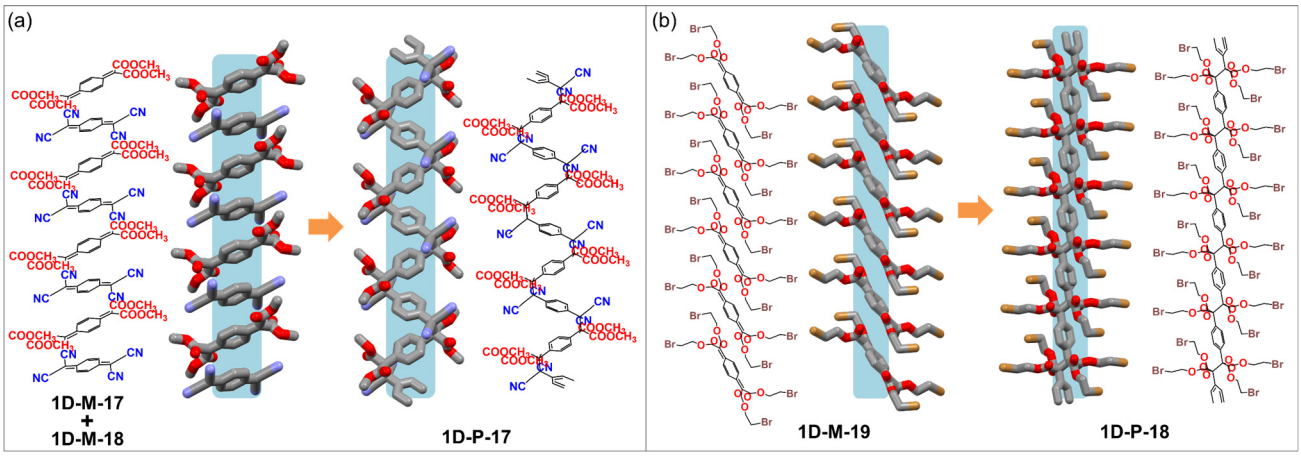

Fig. 10 The chemical and single-crystal X-ray structures of (a) **1D-M-17, 1D-M-18** and **1D-P-17**; (b) **1D-M-19** and **1D-P-18**.

Polymerization is not limited to single crystals but can also be achieved in highly concentrated solutions or semicrystalline thin films. The alkyl side chains in the monomer structures are found to play an important role in molecular packing. The perfect alignment of the monomers in the crystals and the short distance of the two active carbon atoms (~3.2 to ~3.3 Å) are necessary to ensure the occurrence of the topochemical reactions.

Besides the topochemical 1,3-polymerization of a diene, the 1,6-polymerization of a triene can also realize the transformation in a single crystal state. Lauher and Fowler reported a successful example of topochemical 1,6-polymerization of a triene-based monomer **1D-M-16** (Fig. 9e).[127] The π-π stacking of the adjacent pyridine rings in the structures plays a role in determining the stacking modes. The 1-6 carbon-carbon atom distance of adjacent trienes is 4.09 Å, which is a little long for topochemical diene polymerization. However, thermally induced polymerization of **1D-M-16** single crystal resulted in a smooth transformation to **1D-P-16.** The X-ray crystal structure determination clearly demonstrated that a topochemical 1,6-polymerization of the triene **1D-M-16** to a polytriene**1D-P-16** had occurred (Fig. 9e).

1.3.4 Polymerization of quinodimethane

Itoh and co-workers developed the topochemical polymerization of quinodimethane derivatives. They first realized the copolymerization of **1D-M-17** and **1D-M-18** in the single crystal state (Fig. 10a).[128] An orange-colored single-crystal charge-transfer complex of (**1D-M-17** and **1D-M-18**) was successfully obtained due to the electron-donating and electron-accepting behavior of these two monomers. The interplanar distance between **1D-M-17** and **1D-M-18** is 3.38 Å, which meets the requirement for the topochemical polymerization. The subsequent UV light irradiation (high-pressure Hg lamp in vacuo for 18 hours) or heating in the dark (60 °C in vacuo for 3 hours) yields colorless or pink alternating copolymer single crystal (**1D-P-17**) with a *cis* conformation through successive bond formation between reactive exomethylene carbon atoms.

The same group subsequently reported another example of the quinodimethane-based SCP (Fig. 10b).[86] The yellow platelet monomer single crystals (**1D-M-19**) can be easily obtained through recrystallization. However, UV irradiation or heating can only lead to low-quality polymer crystal which is not suitable for the SCXRD. The ^{60}Co γ-radiation with higher energy and better penetration ability was thus utilized for the polymerization in the single-crystal state, which is expected to induce the polymerization rapidly and homogeneously and to provide polymer crystals with fewer defects. After ^{60}Co γ-radiation of 5 kGy at 30 °C for 1 week, the yellow platelet monomer single crystals (**1D-M-19**) were converted to crack-free colorless, transparent polymer single crystals (**1D-P-18**). The SCXRD reveals that the monomer molecule forms a columnar structure, and the polymerization takes place along this column structure, where almost no large displacement of the center of mass is observed before and after the polymerization (Fig. 10b).

1.3.5 Polymerization of diacetylenes and triacetylene

In 1969, Wegner discovered the topochemically controlled 1,4-polymerization of diacetylenes by heating or photo-irradiation.[129] Subsequently, Wegner and Baughman elaborated that the appropriate arrangement of the diyne monomers controls their reactivity, leading to ordered topochemical polymerization.[21] However, in most cases, the diyne monomers do not align properly for 1,4-polymerization on their own. The key factor thus becomes how to control the appropriate alignment of the monomers in the solid state at a distance commensurate with the repeat distance in the target polymer. The solution to this problem could be found in the field of supramolecular chemistry.[129-139] The weak supramolecular interactions become an ideal choice for the modulation of the monomers' self-assembly.[88, 140-149] Goroff and co-workers prepared single-crystal poly(diiododiacetylene) (**1D-P-19**), a nearly unadorned carbon chain substituted with only single-atom iodine side groups by using a co-crystal scaffolding strategy (Fig.11a).[150] A Lewis-base bis(nitrile) oxalamide was used as a host to form co-crystals with the monomer diiodobutadiyne (**1D-M-20**). An appropriate arrangement was successfully acquired through the hydrogen-bonding

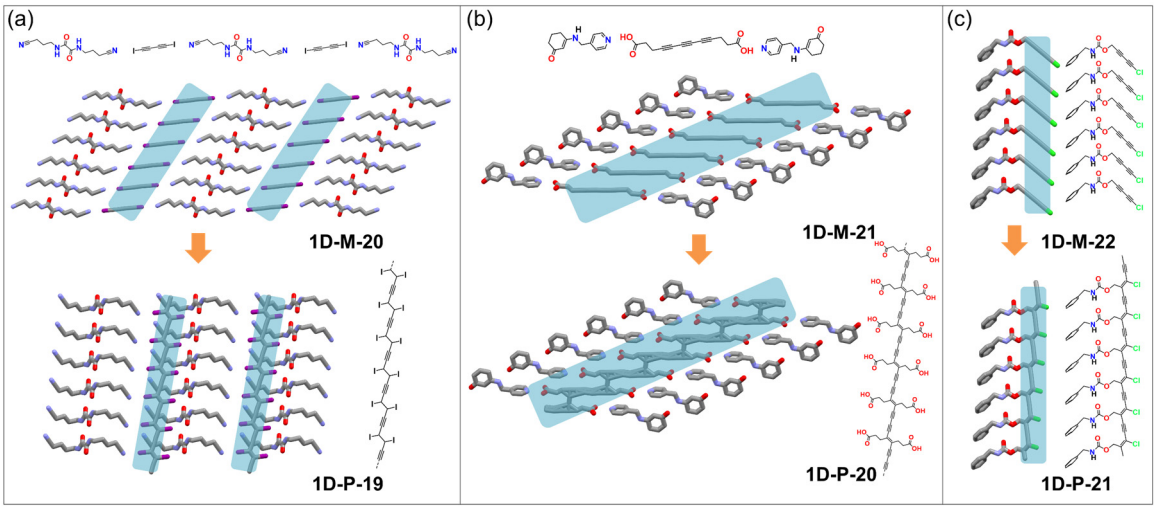

Fig. 11 The chemical and single-crystal X-ray structures of (a) **1D-M-20** and **1D-P-19**; (b) **1D-M-21** and **1D-P-20**; (c) **1D-M-22** and **1D-P-21**.

interactions between the oxalamide groups and weak halogen-bonding interactions between nitriles and iodoalkynes. In the co-crystals with oxalamide as the host, the **1D-M-20** undergoes spontaneous topochemical polymerization to form **1D-P-19** through an SCSC conversion.

Flowler and Lauher reported a 1,6-polymerization of a triacetylene monomer (**1D-M-21**) in a single crystal state through a host-guest co-crystal strategy.[90] As shown in Fig. 11b, a pyridine-based host and carboxylic acid-based triacetylene as monomer was co-crystallized to form a 2:1 complex. The hydrogen-bonding interactions between the carboxylic acid groups from the monomers and the pyridines from the host molecules realize the approximate arrangement of **1D-M-21** with a reasonable reactive distance. The subsequent γ-radiation resulted in 70% completion of the polymerization. The further irradiation brings a sudden phase change in the crystals to an amorphous state.

Besides the additional introduction of the host molecules for the regulation of the monomer alignment, the self-assembly of the monomers themselves can also realize an ideal stacking arrangement through the various supramolecular interactions.[129-142] Baillargeon and co-workers reported a topochemical polymerization of chlorodiacetylene (**1D-M-22**) to afford SCXRD structure determination of polychlorodiacetylene (**1D-P-21**) (Fig.11c).[89] The amide groups in the monomers provide the intermolecular hydrogen bonding interactions of **1D-M-22** for the appropriate alignment of the monomers, thus leading to successful polymerization.

The topochemical polymerization of diacetylenes or triacetylene can lead to 1D conjugated organic polymers, which may exhibit intriguing electronic and optical properties. The unique advantage of this reaction shows great potential in preparing electronic devices, which cannot be realized through other types of topochemical polymerizations. It is worth noting that the preparation of the poly-diyne through topochemical polymerization usually needs a higher energy source. In some cases, the γ-radiation is necessary.

1.3.6 Topochemical azide-alkyne and azide–ene cycloadditions

Topochemical reactions have shown significant advantages in the formation of products in an ordered (crystalline) form. However, reactions that can be done topochemically, especially in a single crystal state, are still limited. Sureshan and co-workers developed a new topochemical azide-alkyne and azide-ene cycloaddition reactions, which can realize the SCSC transformation process. The azide and alkyne or ene groups in the monomers can undergo 1,3-dipolar cycloaddition in the crystal lattice to yield 1,4- or 1,5-disubstituted 1,2,3-triazole or triazoline products. Triazole or triazoline-linked 1D SCPs were thus formed. Around 10 examples of 1D SCPs have been successfully obtained through these topochemical cycloadditions. We have summarized most of these 1D SCPs examples in Fig. 12, including the chemical structures of monomers and polymers and the transformation process in the single-crystal state.[93, 95-98, 151-158] In general, hydrogen-bonding interactions, such as O–H···O, N–H···O, and N–H···N, are the main noncovalent driving force for aligning azide and alkyne or ene-substituted derivatives in orientations suitable for their proximity-driven cycloaddition reaction in crystals. The arrangement of azide and alkyne or ene. Carbohydrates (**1D-P-22**, **29**, **30**), nucleosides (**1D-P-23**), and peptides (**1D-P-24**, **25**, **26**, **27**, **28**, **31**, **32**, **33**, **34**) have been successfully exploited for their topochemical azide-alkyne and azide-ene cycloadditions. Thermal activation is the main driving force for the topochemical cycloadditions. Depending on the activation barrier in each case, the cycloaddition reaction can happen spontaneously at room temperature (or even at lower temperatures) or necessitate heating of the single crystals.

In summary, the "click" reaction has shown widespread adoption in various scientific and industrial contexts due to its high efficiency, versatility, and robustness. The discovery by Sureshan and co-workers verified that the widely used "click" reaction can also undergo a topochemical process in a single crystal state and provide triazole or triazoline-linked 1D SPC products. This reaction can be implemented in diverse molecular categories and has a high potential to enrich the variety of the 1D SCPs.

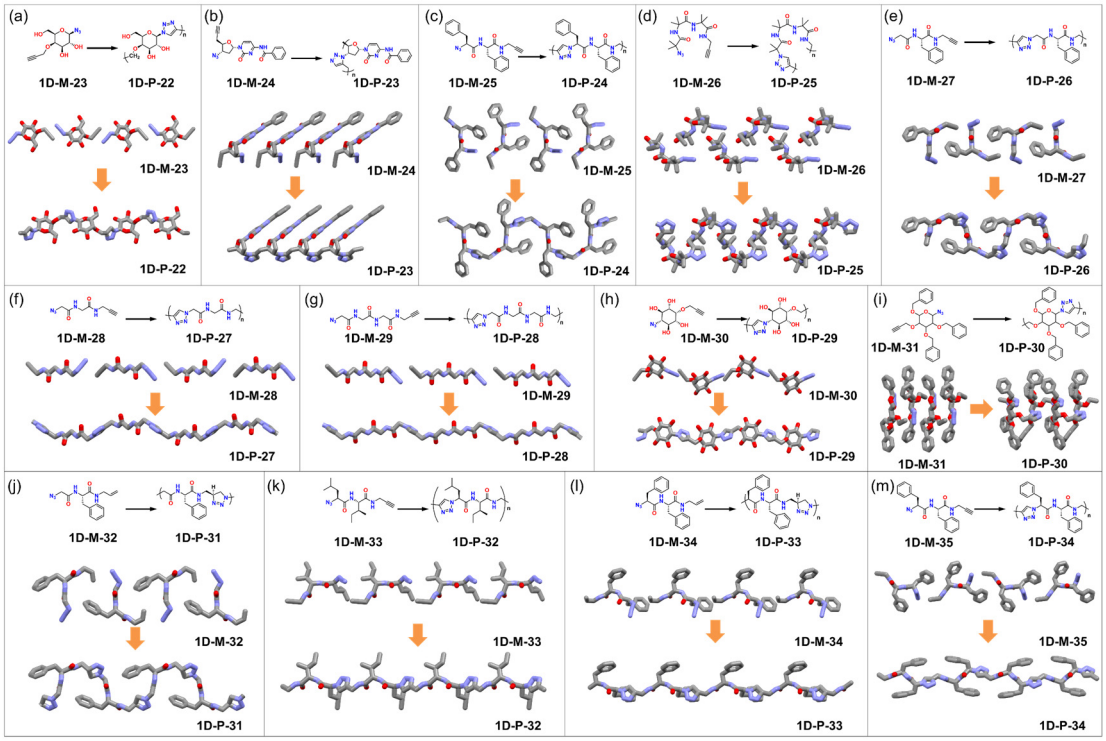

Fig. 12 The chemical and single-crystal X-ray structures of **1D-M-23** to **35** and **1D-P-22** to **34**.

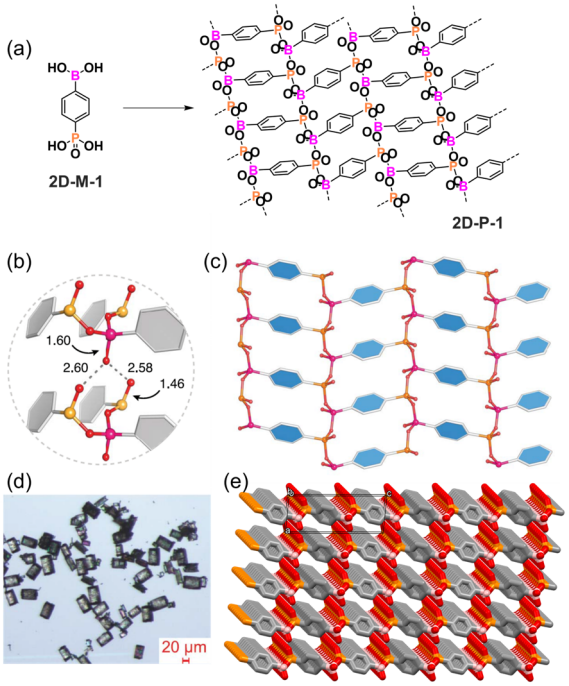

Fig. 13 Solution-based synthesis of single-crystal 2D COFs. (a) The synthesis of **2D-P-1**. (b) The H-bonding formation of each layer. (c) Single-crystal X-ray structure of **2D-P-1** in one layer. (d) Optical microscope image of **2D-P-1**. (e) The packing mode of **2D-P-1** in a single crystal. Reproduced with permission from ref. 167, Copyright 2020, American Association for the Advancement of Science.

2. 2D Architectures

The planar nature of 2D architectures can limit their solubilities, making it challenging to obtain single crystals through recrystallization from polymer solutions, as seen in 1D polymer cases. For a long time, researchers have wondered if highly ordered and covalently linked 2D architectures can be made in a laboratory, even though such structures exist in nature, such as crystalline graphite made of 2D graphene layers. However, recent advancements in 2D architecture synthesis have shown promising results in the creation of these types of structures. In 2005, the first crystalline 2D COF material was successfully prepared by Yaghi via the solvothermal method in solution.[4] This breakthrough discovery has opened up a new era of 2D crystalline polymers, and since then, thousands of 2D COF materials with diverse structures have been designed and synthesized in solution.[5, 16, 44-46, 159] The reversible covalent bond is necessary for the formation of highly ordered structures. Compared to crystalline hydrogen-bonded organic framework (HOF) materials or coordination-bonded metal-organic framework (MOF) materials, COFs are typically more challenging to crystallize.[160-166] Most of the reported COF materials are polycrystalline powders. The structure characterization has been limited to the analysis of PXRD combined with computer simulation modelling. Despite the challenges involved in achieving the atomic-level definitive structures through SCXRD, there have been remarkable breakthroughs in the synthesis of 2D COF single crystals from solutions.

2.1 Solution Synthesis

Yaghi and co-workers designed a simple organic linker **2D-M-1** consisting of boronic acid and phosphonic acid groups (Fig. 13a).[167] Through a simple molecular dehydration reaction, a single crystal of 2D layered COFs with a rod unit of an infinite valency structure was obtained, which was referred to as

"infinity" (rods) in this study. The single crystals of **2D-P-1** had a block shape (Fig. 13d). The SCXRD structure analysis showed the 1D B–O–P rods consist of alternating tetrahedral boron and phosphorus groups (Fig. 13c, e). These rods were connected by phenylenes, forming a 2D structure with an interlayer spacing of 5.47 Å (Fig. 13b). The layers were stacked along the *a* axis and arranged in a honeycomb pattern.

Generally, 2D COFs have been obtained as polycrystalline solids with a small crystalline domain size. This could be attributed to the poor control of the nucleation process. Currently, the formation mechanism of 2D COFs remains poorly understood, and the influence of the reaction rates and defect repair process is still largely unknown. Dichtel and co-workers have conducted mechanistic studies on the boronate ester-linked 2D COFs.[168] They found that the nucleation-elongation process was crucial for the growth of the single-crystal COFs (Fig. 14). However, this process is usually disturbed by the precipitation and aggregation of COF microcrystals. A two-step approach is adopted that separates the nucleation and growth processes. A second growth step in which additional monomers were introduced slowly suppressed the further nucleation. The COF colloids can be enlarged into faceted single crystals with lateral dimensions greater than 1.5 µm. Preventing premature precipitation and aggregation of the microcrystalline COF could help stabilize the colloidal suspensions of single-crystalline boronate ester- and boroxine-linked 2D COF nanoparticles, thus improving the crystalline quality of the products.[168]

Dichtel and co-workers found that this colloidal suspension method was also applicable to imine-linked COFs.[169] Micron-sized single crystals of two 2D COFs (**2D-P-2** and **2D-P-3**) were successfully synthesized by using a Schiff base reaction within as little as 5 min (Fig. 15a). The nitrile-containing solvent was used with aniline as a monofunctional modulator and benzoic acid as a catalyst. Large crystals, 4 µm-wide squares of **2D-P-2,** and 20 µm-sized hexagons of the **2D-P-3** were obtained by varying the crystallization conditions (Fig. 15b-h). Besides the traditional PXRD characterization, continuous rotation electron diffraction (cRED) was used to elucidate the unit cells of **2D-P-2** and **2D-P-3** single crystals (Fig. 15j-m). Relatively accurate structure models were obtained by the Rietveld refinement. They also proposed that a possible slip-stack happens along the *c*-axis to minimize the free energy.

Zhao and co-workers obtained a single crystal of 2D COF (**2D-P-4**) (Fig. 16a), which has the same chemical structure as **2D-P-2**.[170] As shown in Fig. 16a, **2D-M-6** was chosen because the aniline-protected aldehyde groups can react with the amine groups of **2D-M-2** at a much lower rate than the unprotected aldehyde groups in **2D-M-7**. This provides sufficient time for the pre-arrangement of monomers and oligomers to facilitate crystal growth. Rhombus plate-like single crystals with a size of 2-5 µm were obtained after 30 days of growth (Fig. 16b, c). The authors speculated that the monomers and oligomers go through self-assembly and pre-arrangement process before the polymerization. Thus, the pyrene-based **2D-M-2** (Fig. 16a) is likely preferred over the benzene core for single crystal growth because the large π-conjugated planar structure would likely enhance inter-molecular binding interactions. The crystal

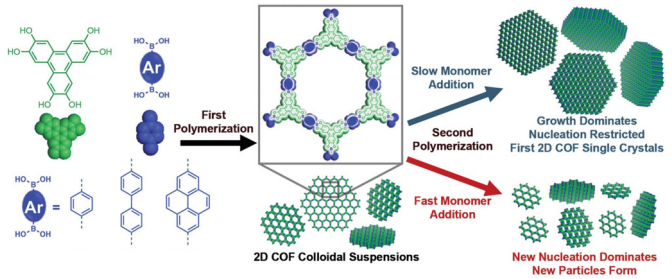

Fig. 14 Schematic of controlled 2D polymerization through a two-step seeded growth approach. Reproduced with permission from ref. 168, Copyright 2018, American Association for the Advancement of Science.

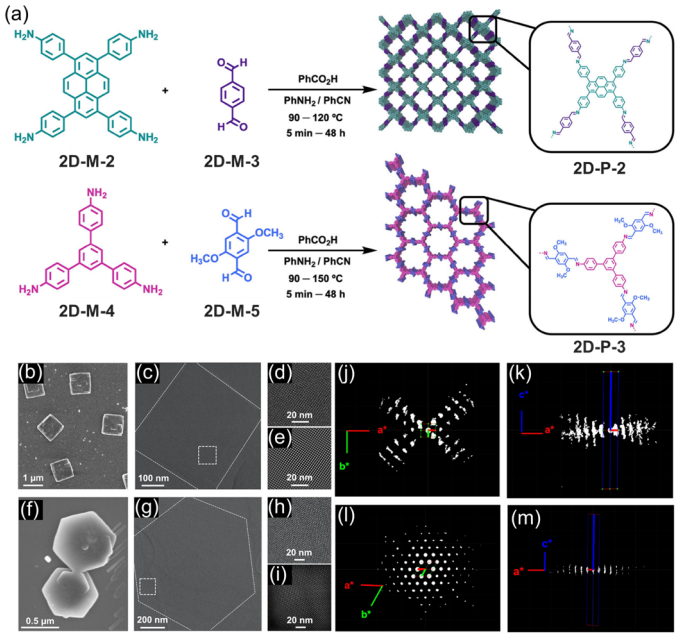

Fig. 15 Solution-based synthesis of single crystal 2D COFs: (a) Synthesis of **2D-P-2** and **2D-P-3**. (b) SEM and (c, d, e) HRTEM images of **2D-P-2** single crystals. (f) SEM and (g, h, i) HRTEM images of **2D-P-3** single crystals. (j, k) 3D reciprocal lattices of the **2D-P-2** at 4.4 Å resolution and (l, m) **2D-P-3** at 4 Å resolution, as determined by low-dose cRED. Reproduced with permission from ref. 169, Copyright 2022, American Chemical Society.

structure of **2D-P-4** was successfully characterized by cRED with a resolution of 0.76 Å (Fig. 16d-f). Interestingly, only 10% of the crystals adopt the widely predicted AA stacking structure (Fig. 16g, h). The remaining 90% of the crystals have a previously unknown stacking structure, containing 6 stacking layers within one unit cell. Unfortunately, this unknown single-crystal structure could not be resolved due to its high complexity.

Although the above examples of single-crystal 2D COFs reported by the Dichtel and Zhao groups were obtained under different reaction conditions and the research goals are also different, both results indicate the possibility of diverse stacking along the *c*-axis in the pyrene-based 2D COFs. In fact, the synchronized offset stacking in 2D COFs has been well investigated previously by Bein and co-workers.[171, 172] The consecutive COF sheets can be locked in position during crystal growth, thus minimizing the occurrence of stacking faults and dislocations. The propeller-shaped molecular building units, such as tetraphenylethylene and triphenylamine, or pyrene units with substituents on the core, can generate well-defined periodic docking sites, which guide the assembly of successive

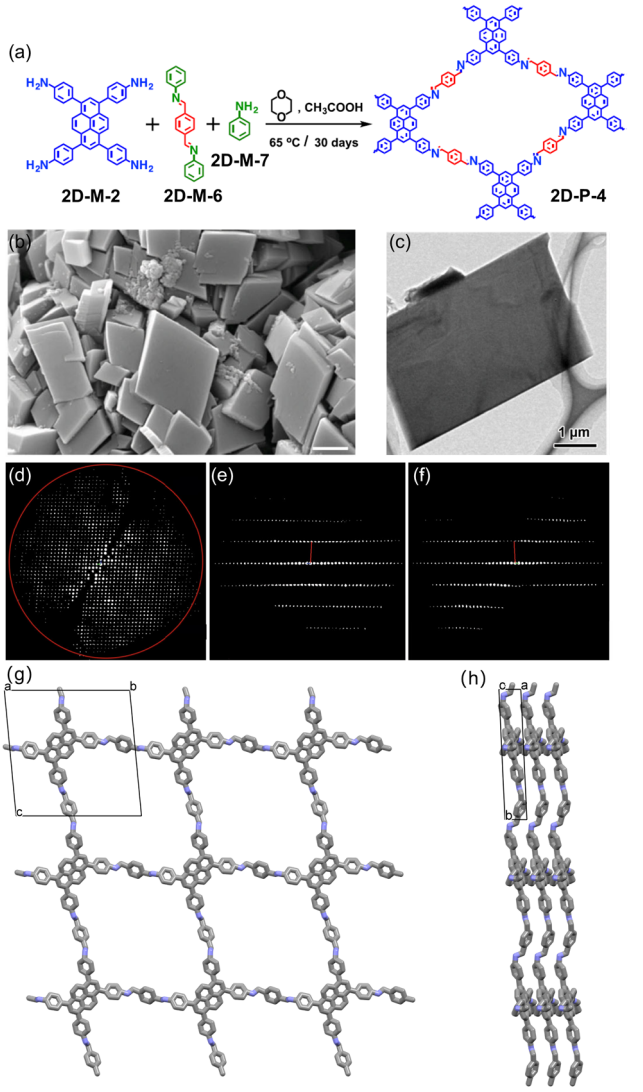

Fig. 16 Examples of solution phase synthesis of single crystal 2D COFs: (a) Synthesis of **2D-P-4**; (b) SEM image of **2D-P-4** crystals; (c) TEM image of **2D-P-4** crystals; (d)-(f) 3D reciprocal lattice of **2D-P-4** reconstructed from the cRED data viewing along the (d) [100], (e) [010], and (f) [001] directions. (g) Single crystal structure of **2D-P-4** (view from c-axis). (g) Single crystal structure of **2D-P-4** (view from *b*-axis). Reproduced with permission from ref. 170, Copyright 2022, Springer Nature.

layers. As a result, the long-range ordered stacking was promoted during the COF formation.

2.2 Topochemical polymerization

As discussed previously, confining the polymerization within a 2D plane and creating long-range order along the *c*-axis through stacking in solution could be challenging. In this context, SCSC transformation provides a viable alternative, which involves the preorganization of monomers in a crystal lattice and their polymerization in the solid state. Similar to the 1D SCPs cases, this approach requires a proper packing of monomers with a specific orientation of reactive sites in each layer so that the polymerization can occur later between monomers within the 2D layer and form 2D SCPs. However, the control of crystal packing of monomers in the desired manner is challenging. It has been mainly based on chemical intuition and the continuous trial-and-error process, which frequently leads to undesired packing motifs. Additionally, during the SCSC transformation, cracking of the single crystal sometimes happens because of the lattice contractions or expansions during the polymerization process, which can also make SCXRD analysis not feasible. Although there have been many challenges in such a process, researchers have achieved several successful examples of 2D SCPs through topochemical polymerization.

In 2009, Schlüter raised an interesting question: "Two-dimensional polymers: just a dream of synthetic chemists?"[173] The synthesis of these polymeric materials, which are atomic thin, covalently bonded, and in long-range order, represents a grand challenge. In 2014, Schlüter and co-workers reported the first successful synthesis of a 2D SCP through SCSC.[9] The rotor-shaped anthracene-based monomer **2D-M-8** is composed of three anthracenes as blades (Fig. 17b). The packing behavior of the solvent for growing the crystal. After many attempts, **2D-M-8** in solid state (single crystals) was highly dependent on cyanopyridine was finally found to be a suitable solvent in which a face-to-face arrangement of anthracene units was achieved (Fig. 17c). A model study was conducted using a simple anthracene derivative, which confirmed the feasibility of such an approach (Fig. 17a). A successful formation of the extended 2D network with an interlayer distance of around 3.6 Å was then followed. In detail, the monomer single crystals with sizes >200 μm were irradiated for 48 hours with blue light (465 nm) to form **2D-P-5** via [4 + 4] photo-cycloaddition (Fig. 17d). The size of **2D-P-5** is dependent on the monomer single crystal grown from the solution. Both the exact structures of the monomer **2D-M-8** and the obtained **2D-P-5** were confirmed by regular SCXRD analysis.

During the same period, King and co-workers also independently designed a triptycene-based monomer (**2D-M-9**) which contains three anthracene moieties as blades (Fig. 17e).[80] Every "blade" contains four fluorine atoms at the outer rim of the anthracene. By using the same [4+4] cycloaddition chemistry, a similar 2D SCP was obtained. The single crystal of the monomer **2D-M-9** was grown in chloroform, which has a 2D layered packing based on SCXRD. Each layer consists of **2D-M-9** monomers stacked facing each other in a quasi-hexagonal packing arrangement (Fig. 17f). The blue light (400-460 nm) triggered the [4 + 4] photo-dimerization, which led to the SCSC transformation to yield a 2D SCP **2D-P-6** (Fig. 17f). Notably, an intermediate dimer crystal was observed during the early stage of photopolymerization (460 nm) in the single crystal state. The **2D-P-6** single crystal was obtained after elongated ultraviolet irradiation (400 nm) of the dimer crystal at 223 K (Fig. 17f). These pioneering works in the preparation of 2D SCPs have received significant scientific attention,[9, 80] and opened new possibilities for making 2D SCPs by controlling the growth of single crystals of well-designed monomers rather than controlling the polymerization conditions (conventional approach).

Besides the [4 + 4] photo-dimerization of anthracenes in a solid state for making the 2D SCPs, the [2 + 2] cycloaddition was also successfully applied in the SCSC process. Schlüter and co-workers designed a pyrylium-based triolefinic monomer **2D-M-10** (Fig. 18a).[174] A single crystal of **2D-M-10** was obtained in a mixture of acetic and formic acids. Monomer **2D-M-10**

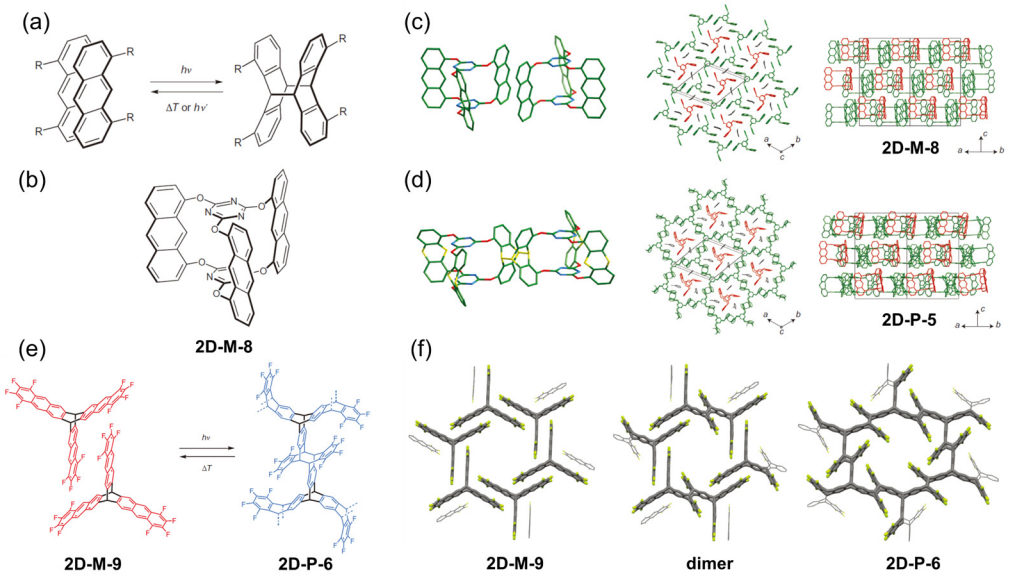

Fig. 17 The pioneering topochemical polymerization approaches to obtain 2D SCPs: (a) A model reaction of the photochemical dimerization of anthracenes derivatives. (b) Molecular structure of **2D-M-8**; (c) The crystal structure and the packing mode of **2D-M-8**; (d) The crystal structure and the packing mode of **2D-P-5**; (e) Structures of **2D-M-9** and the corresponding **2D-P-6**; (f) The crystal structures of the **2D-M-9** and the corresponding **2D-P-6**. Reproduced with permission from ref. 80 and ref. 173, Copyright 2014, Springer Nature.

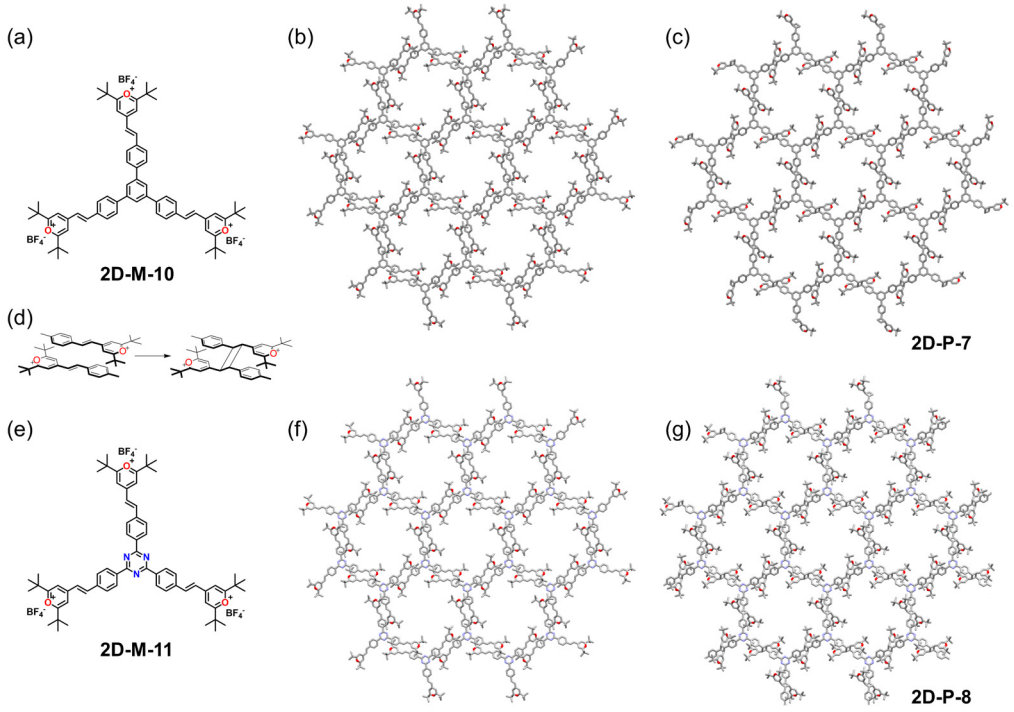

Fig. 18 Topochemical polymerization approach to obtain 2D SCPs through [2+2] cycloaddition: (a) Structure of **2D-M-10**; (b) Single-crystal structure of one layer of **2D-M-10**; (c) Single-crystal structure of one layer of **2D-P-7**; (d) Dimerization of the model compound; (e) Chemical structure of **2D-M-11**; (f) Single-crystal structure of one layer of **2D-M-11**; (g) Single-crystal structure of one layer of **2D-P-8**.

crystallized into a layered structure with a distance of 3.9 Å between the neighboring olefin moieties of **2D-M-10** (Fig. 18b), which meets the Schmidt criterion for the topochemical reaction.[175]

Irradiation (530 nm) at 4 °C induced a color change of the crystals from orange to yellow, indicating the interrupted conjugation and the occurrence of polymerization. A novel 2D polymer (**2D-P-7**) with pyrylium units was formed upon the completion of the polymerization. As shown in Fig. 18c, six pyrylium units point inside each pore of **2D-P-7**, fully decorating the pores with positively charged pyrylium groups. This feature may endow the novel 2D polymer with excellent polyelectrolyte properties.

Zhao and co-workers reported another example of a 2D SCPs

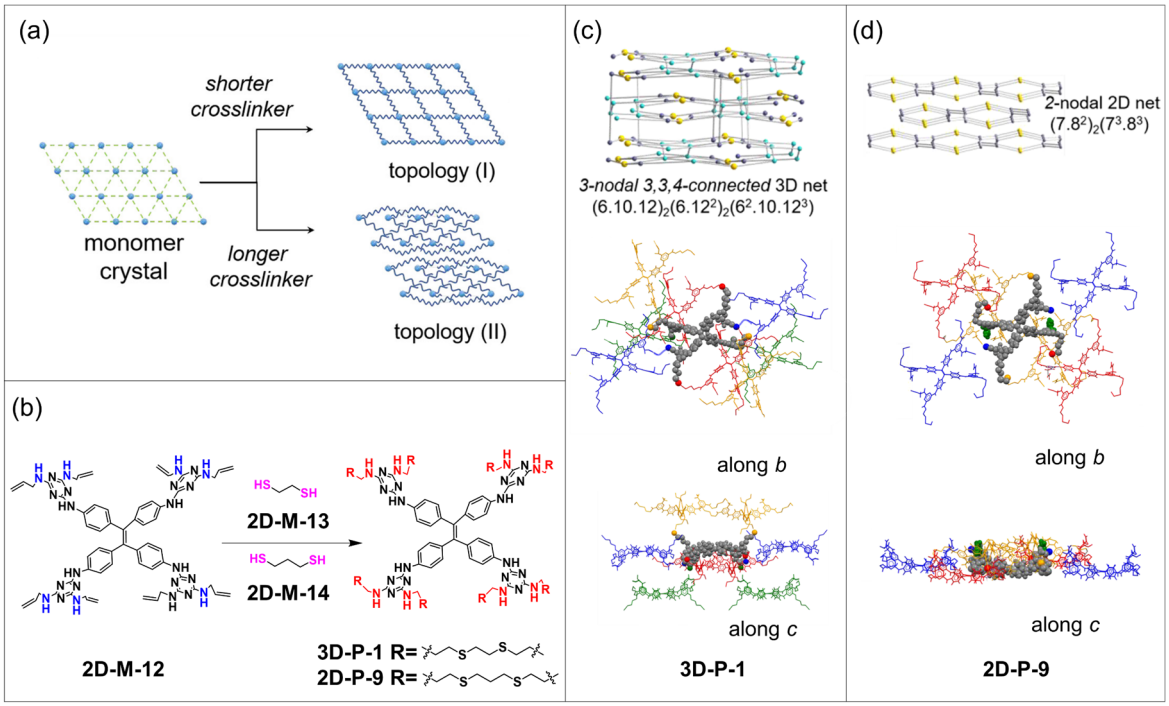

Fig. 19 Topochemical crosslinking of monomers with flexible linkers: (a) Schematic representation of the synthesis of H_COFs materials; (b) Synthesis of **3D-P-1** and **2D-P-9**; (c) The topology and single-crystal structure of **3D-P-1**. (d) The topology and single-crystal structure of **2D-P-9**. Reproduced with permission from ref. 177, Copyright 2019, American Chemical Society.

through SCSC transformation using monomer **2D-M-11**, which is similar to monomer **2D-M-10** (Fig. 18e).[176] Triazine was used as the core instead of the benzene ring. Fortunately, the structural alteration does not cause a significant change in the crystal packing of **2D-M-11** compared to monomer **2D-M-10**. In **2D-M-11**, three arms were packed head-to-tail to form a hexagon (Fig. 18f). Given the distance between neighboring styryl units (3.919 Å), the [2 + 2]-photo-cycloaddition could take place. Upon irradiation with 530 nm light for 12 hours, the crystal underwent a color change from dark yellow to light yellow, while still maintaining the translucent feature. SCXRD confirmed the successful polymerization and the formation of a 2D polymer (**2D-P-8**). The hexagonal honeycomb porous structures were formed in each layer with a pore diameter of 2.7 nm (Fig. 18g). Notably, it was found that a minor change in the monomer structure could play a critical role in the layer exfoliation process. The addition of CF_3COOH (TFA) led to the protonation of the triazine core and introduced repulsive forces between layers due to charge and/or steric effects, thus facilitating the exfoliation process. More than 60% of the monolayered 2D polymer was found in a clear solution-like sample in TFA/gamma-butyrolactone (GBL).

All the examples mentioned above involve the topochemical polymerization of a single type of rigid monomer. Simultaneous integration of the features with high flexibility and high crystallinity into porous polymers is particularly challenging. Ke and co-workers reported a series of single-crystal organic frameworks crosslinked by H-bonds, which are named hydrogen-bonded cross-linked organic frameworks (H_COF). The flexibility and crystallinity are integrated into a single framework of H_COF (Fig. 19).[177] Similar to the topochemical polymerization, it is necessary to preorganize the monomers through H-bonding interactions.[160, 178] Subsequently, a second component, such as alkyldithiols, was introduced as flexible crosslinkers. The single crystals were photo-polymerized via thiol-ene or thiol-yne reactions through SCSC transformation.

As shown in Fig. 19a and b, monomer **2D-M-12**, containing tetraphenylethylene core with four melamine units and eight allyl groups, was designed and synthesized. A single crystal of monomer **2D-M-12** was obtained through slow vapor diffusion of MeCN into DMF solutions. Subsequently, flexible alkyldithiols with different lengths (**2D-M-13**, **2D-M-14**) were introduced into the monomer crystal as the crosslinkers through diffusion. UV irradiation yielded **3D-P-1** and **2D-P-9**. SCXRD analysis showed that **2D-P-9**, which was synthesized with a short crosslinker, formed a 2D network, whereas **3D-P-1**, which was synthesized with a longer crosslinker, formed a 3D interconnected network (Fig. 19a). As shown in Fig. 19c and d, **2D-P-9** is a 2-nodal 3,4-connected 2D network in which two neighboring layers of the monomer **2D-M-12** are covalently crosslinked and extended along the [010] plane. By contrast, **3D-P-1** is an interconnected 3D network exhibiting a 3-nodal 3,3,4-connected self-entangled structure.

The same group subsequently reported another 2D SCP through a similar strategy.[179] As shown in Fig. 20a, a 2D hexagonal H-bonded structure was first formed via a co-crystallization of **2D-M-15** and **2D-M-16**. **2D-P-10** was then obtained via an SCSC transformation through the thiol-ene crosslinking (Fig. 20a). The heteromeric co-crystallization of two COOH-based monomers led to a suitable packing mode of the crystal, allowing the subsequent thiol-ene reaction. In **2D-P-10**, the dithioether linkage A was found to connect **2D-M-15** in non-

adjacent 1,4-layers, while the linkages C and D connect two allyl groups in 1,3-layers (Fig. 20b, c). The linkage B connects 1,2- and 1,3-layers, forming 2D structure with flexible interlayer cross-linkages. This example showcases an interesting strategy for achieving the desired packing of monomers with the positioning and orientation necessary for interlayer crosslinking to form 2D polymers through co-crystallization using a complementary set of monomers.

Ke and co-workers recently reported 2D porous single crystals that are formed from a three-arm monomer (**2D-M-17**) consisting of piperazine and diallylmelamine moieties (Fig. 21a).[180] Due to piperazine's semi-rigid chair conformation, the π–π interactions between stacked layers in the solid state are reduced. The assembly of **2D-M-17** with an anion, HSO_4^-, formed porous single crystals with unique tris-anion $(HSO_4^-)_3$ clusters. The subsequent thiol-ene SCSC transformation through photo-irradiation covalently crosslinked the allyl groups in the preorganized molecular crystal, forming a 2D SCP (**2D-P-11**) with large voids (Fig. 21c). Notably, **2D-P-11** exhibited rapid and reversible size expansion and contraction (>200%) upon a guest uptake and switching between crystalline and amorphous phases due to the guest-induced disruption of the anion cluster.

These studies hold great promise for achieving both high crystallinity and flexibility in organic frameworks. Achieving the optimal balance between rigidity and flexibility while keeping the single crystal state before and after the reaction is the critical factor for the success of HcOF single crystals formation. So far, the reaction to form the H_COF is limited to the topochemical thiol–ene cycloaddition, which requires vinyl group in the parent molecules and thiol groups in the flexible crosslinkers. The concept of a rigid-flexible combined strategy has proven to be effective in the construction of 2D SCPs. By introducing second components as crosslinkers to covalently connect the parent molecules in an SCSC manner, the need for extremely strict 2D packing mode for the monomers in the single-crystal state, as in the single-component topochemical polymerization, could be avoided. Guest-induced changes in the void structure of H_COF could have intriguing applications in selective adsorption and release of guests with high capacity.

2.3 Other approaches

As is well known, the key to 2D graphene preparation is obtaining the monolayered graphene, which is normally obtained through the exfoliation of the bulk graphite.[3] The advantages of the 2D structure are most evident in the case of monolayered graphene. Similar to the production of monolayered graphene, the preparation of a monolayer 2D polymer undoubtedly represents a grand challenge in this field.[176, 181] It is now possible to obtain large-sized 2D SCPs in a synthesis lab, but controlling the exfoliation process to achieve a monolayer with a good dispersity through the so-called "top-down" strategy presents a significant challenge.[176, 182-188] An alternative approach to preparing monolayered, large-sized, and free-standing 2D polymers is through "bottom-up" interfacial synthesis. Such an approach takes advantage of the template and confinement effect of an interface, allowing for

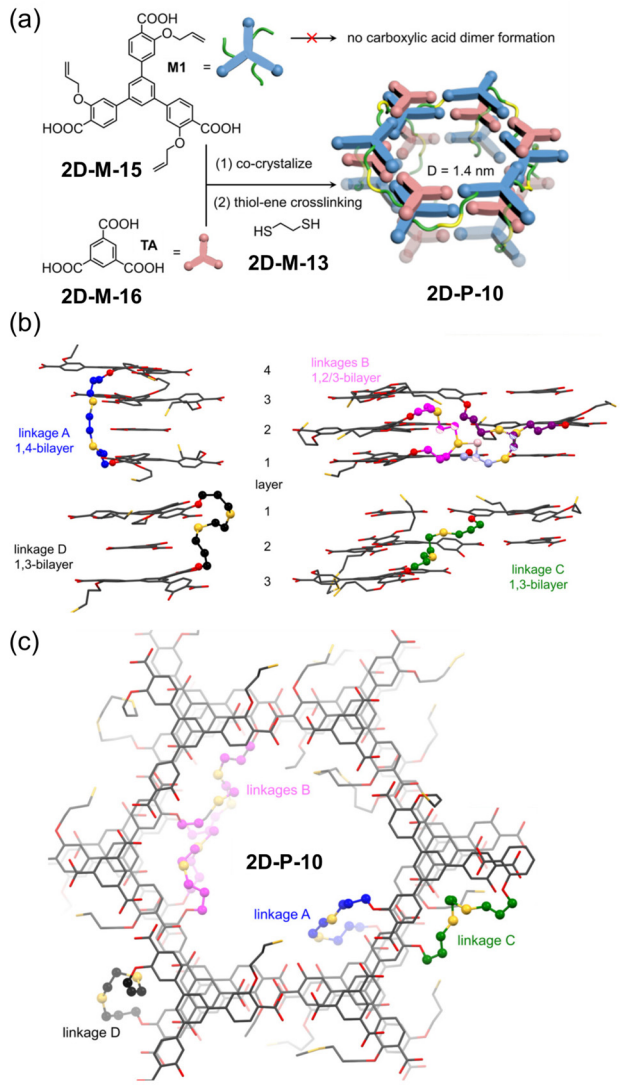

Fig. 20 Layered packing of monomers enabled by co-crystallization and subsequent topochemical crosslinking: (a) Synthesis of **2D-P-10**; (b) Dissected sections of **2D-P-10**; (c) Single-crystal structure of **2D-P-10.** Reproduced with permission from ref. 179, Copyright 2021, Wiley-VCH.

pre-assembling the monomers at an air/water interface to yield a single-crystalline 2D polymer film.[189-193] Although there is no direct evidence from SCXRD or cRED, the structures of these ultra-thin 2D polymers have been assumed well-defined according to the characterization of the selected area electron diffraction (SAED), high-resolution transmission electron microscopy (HRTEM) or high-resolution atomic force microscopy (HRAFM). To date, many crystalline 2D polymer films have been successfully prepared through interfacial synthesis.[192, 194-203] Several excellent reviews have summarized these examples.[173, 193, 204, 205] Thus, they are not covered in detail here.

Just as nature creates 2D graphite or 3D diamond, C_{60}-based SCP has also been obtained under extreme conditions, such as high pressures in the range of several GPa in a laboratory setting.[206-209] High-pressure polymerization of C_{60} has been widely studied through [2+2] cycloaddition.[210, 211] Three polymeric phases, including 1D orthorhombic (O), 2D tetragonal

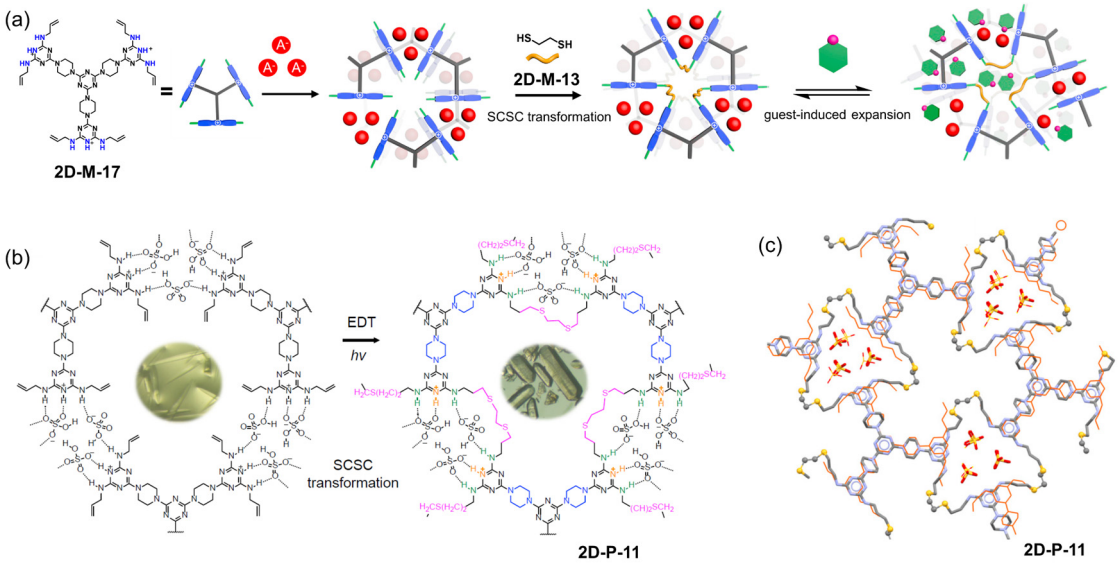

Fig. 21 Crystallization of monomers through ion-cluster formation and their topochemical crosslinking: (a) Illustration of the anion-cluster-directed formation of a hexagonal hydrogen-bonded network, conversion to **2D-P-11** through SCSC crosslinking, and the guest uptake process; (b) Synthesis of **2D-P-11** through thiol-ene SCSC transformation. (c) Single crystal structure of **2D-P-11**. Reproduced with permission from ref. 180, Copyright 2022, Elsevier.

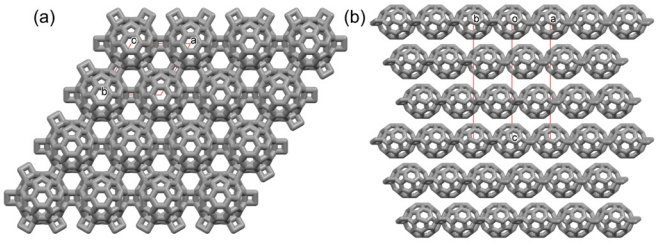

Fig. 22 2D fullerene SCP: (a) Single-crystal structure of monolayer of **2D-P-12**; (b) ABC packing mode of **2D-P-12** in a single crystal.

(T), and 2D rhombohedral (3R) phases, have been reported for these polymers. Yamanaka and co-workers obtained the single-domain crystals of the 3R 2D C_{60} polymer (**2D-P-12**) under high pressure of 5 GPa at 773 K.[206] As shown in Fig. 21a, the crystal structure of **2D-P-12** consists of a hexagonal 2D layered structure formed by the polymerization of C_{60} molecules through [2+2] cycloaddition. The unit cell adopts an ABC stacking mode along the *c*-axis, with the layers held together through van der Waals forces (Fig. 22b).

Since the discovery of the first fullerene C_{60}, the reactivity and different reactions of C_{60} have been widely studied,[212, 213] including the reaction of C_{60} with alkaline earth metals.[214-216] Several single-crystal examples of metal-doped fullerene polymers prepared through vapor-phase growth at normal pressure have been reported.[213, 217-219] For example, Tanaka et al. synthesized a single crystal of Mg-doped 2D fullerene polymers (**2D-P-13**) through a binary vapor-phase mixture of Mg and C_{60} in sealed glass tubes at elevated temperatures (Fig. 23).[220] The mixture was placed in a two-zone furnace with a temperature gradient of 500-600 °C for 24 hours, and the single crystals were obtained in the zone of lower temperature (500 °C). The crystal structure revealed that the C_{60} molecules were connected along the *a* and *b* axis to form a 2D layer, which is stacked along the *c*-axis in an AB stacking mode, with Mg

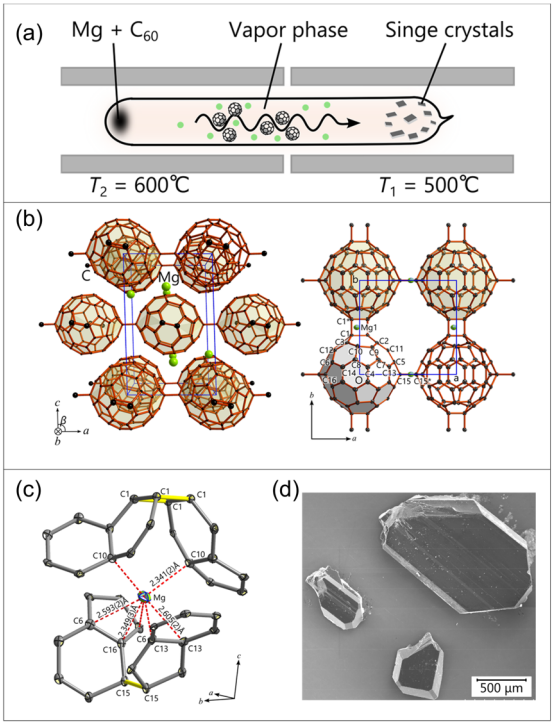

Fig. 23 Mg-doped 2D fullerene SCP: (a) Schematic picture of the equipment for the synthesis of Mg-doped fullerene polymer **2D-P-13**. (b) Single-crystal structure of **2D-P-13**. (c) Carbon coordination surrounding the Mg atom. (d) SEM image of **2D-P-13** single crystal. Reproduced with permission from ref. 220, Copyright 2018, American Chemical Society.

atoms intercalated between the layers at an Mg-C distance smaller than 2.7 Å.

Recently, Zheng and co-workers successfully exfoliated the 2D magnesium-doped C_{60} SCPs using a cation intercalation method.[221] Two different Mg-intercalated single crystals of 2D.

C_{60} polymers with quasi-hexagonal (**2D-P-14**) and quasi-tetragonal (**2D-P-15**) structures were obtained through a facile reaction at atmospheric pressure by adjusting the ratio of Mg and C_{60} (Fig. 24a, b). The subsequent introduction of tetrabutylammonium salicylate (TBAS) cleaved the C–Mg bonds between C_{60} polymer layers and tetrabutylammonium (NBu^{4+}) cations and replaced Mg ions in the interlayer. The larger ionic radius of NBu^{4+} led to an effective expansion of interlayers, facilitating exfoliation (Fig. 24c)

Due to the asymmetric lattice structure derived from the orderly arrangement of asymmetric C_{60} cages, the single layer of **2D-P-15** exhibited in-plane anisotropic behavior, including anisotropic phonon modes and conductivity. With a bandgap of 1.6 eV, the single-layered 2D C_{60} polymer holds great potential for applications in optoelectronics.

3. 3D Architectures

Diamond represents an excellent example of 3D SCPs. Synthetic strategies for 3D SCPs are similar to those used for 2D SCPs, which include solution synthesis, topochemical synthesis, and high-pressure synthesis. It is worth noting that there are more successful examples of solution-synthesized 3D SCPs than 2D SCPs. Conversely, there are more examples of topochemically synthesized 2D SCPs than 3D SCPs. Likely, the growth in 3D orientations may favor the formation of 3D structures in solution, whereas the possible slippage between the layers in 2D SCPs hinders the growth of single crystals. Thus, for 2D SCPs, topochemical synthesis has been more successful than solution synthesis.

3.1 Solution Synthesis

3.1.1 Modulator-assisted synthesis

Wang, Yaghi, and Sun developed a general strategy for the synthesis of large-sized single crystals of 3D COFs.[11] The key step of achieving good crystallinity is the efficient self-correction of defects. The authors envisioned improving the reversibility of the imine bond could facilitate the formation of high-quality crystals. This was accomplished by introducing an excess of aniline, which could act as a competitive modulator and a nucleation inhibitor. The excess aniline could slow down the reaction rates and facilitate the self-correction process. As a result, large-sized single crystals were obtained. Four 3D COF single crystals with uniform blocks (**3D-P-2**, **3D-P-3**, **3D-P-4**, and **3D-P-5**) were obtained by using such modulation strategy (Fig. 25). The large size and high quality of the single crystals enabled unambiguous structure elucidation through SCXRD analysis. The commonly encountered ambiguities of interpenetration in 3D COFs, the location of the guest molecules, the imine bond formation, and the determination of complicated topology were clearly deciphered with atomic resolution, which could not be accomplished by using the common PXRD characterization.

Applying this modulation strategy, Wang and co-workers further reported a non-interpenetrated COF (**3D-P-6**).[222] Quadrilateral and tetrahedral linkers consisting of

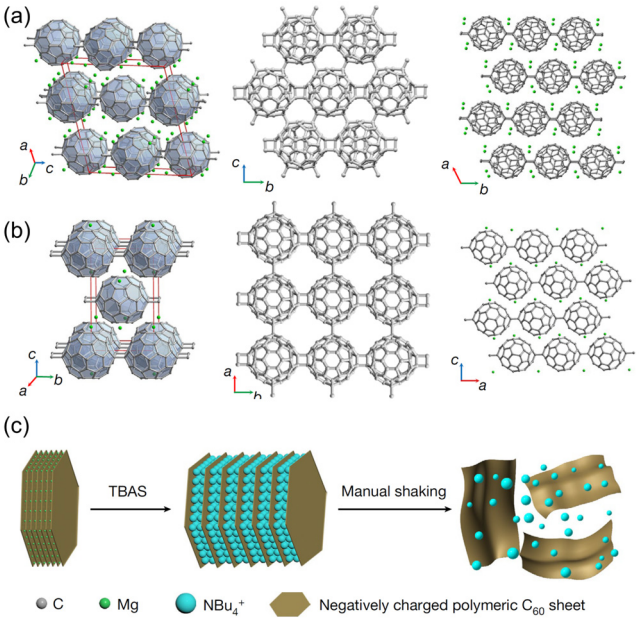

Fig. 24 Exfoliation of 2D fullerene SCP: (a) Single-crystal structure of **2D-P-14**; (b) Single-crystal structure of **2D-P-15**; (c) Schematic of the exfoliation process Reproduced with permission from ref. 221, Copyright 2022, Springer Nature.

tetraphenylethylene and adamantane, respectively, were used as building blocks to construct a single-crystal 3D COF with a new topology and less interpenetration (Fig. 26a). By using the modulation strategy (adding nucleation inhibitor and competitive modulator), single crystals of **3D-P-6** were obtained. SCXRD measurement on a single crystal with a size of 50 μm (Fig. 26d, e) using synchrotron light sources showed the tetragonal unit cell. Further cRED characterization confirmed the unit cell parameters. Based on the SCXRD and diffraction data, a non-interpenetrated open framework with a pts topology was established (Fig. 26b, c).

Wang, Sun, and co-workers designed a new tetrahedral node for constructing 3D COFs by introducing steric hindrance in the ortho positions of biphenyl cores to generate nonplanarity of the monomer (**3D-M-9**). The dihedral angles resulted in the formation of the tetrahedral building unit **3D-M-9** (Fig. 27).[223] The size of **3D-P-7** crystals obtained through conventional solvothermal synthesis was very small. However, when aniline was added as a modulator under optimized conditions, **3D-P-7** with a larger crystal size was successfully obtained, which could be analyzed by cRED with a resolution of 2 Å. The structure analysis showed that **3D-P-7** adopts a 7-fold interpenetrated structure with a pts topology. Although the number of successful examples is still minuscule, the modulation strategy has shown great potential in synthesizing single-crystal 3D COFs with tunable sizes, especially the preparation of large-sized single-crystal 3D COFs for SCXRD analysis.

3.1.2 Conventional solvothermal synthesis

As mentioned previously, conventional solvothermal synthesis typically yields polycrystalline powders instead of high-quality single crystals. Nevertheless, under optimized reaction conditions, the synthesis can yield single-crystal 3D COFs,

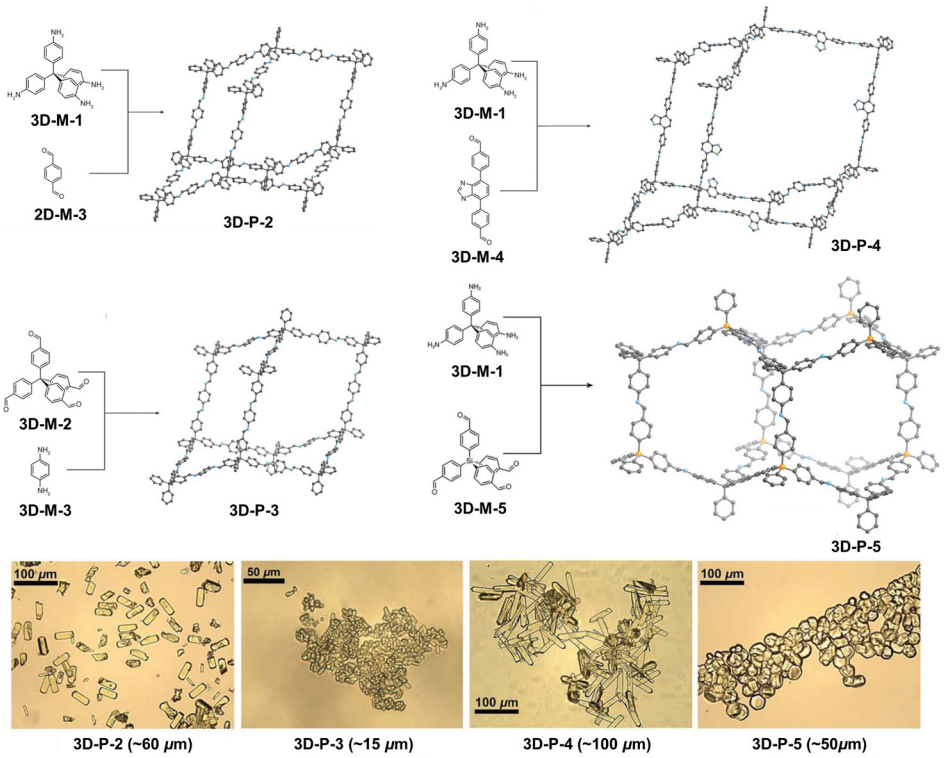

Fig. 25 The synthesis and single-crystal structures of four 3D COFs (**3D-P-2**, **3D-P-3**, **3D-P-4**, and **3D-P-5**) and the corresponding optical microscopy images. Reproduced with permission from ref. 11, Copyright 2018, American Association for the Advancement of Science.

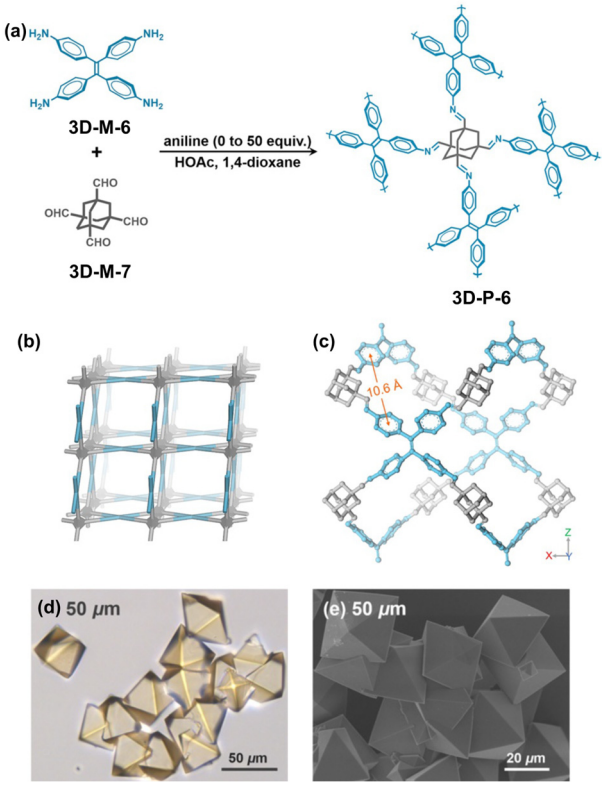

Fig. 26 Non-interpenetrated 3D COF: (a) Synthesis of single-crystal COFs **3D-P-6**; (b) Non-interpenetrated pts topology; (c) Crystal structure of **3D-P-6**; (d) The optical microscopy image of **3D-P-6**. (e) SEM image of single-crystal **3D-P-6**. Reproduced with permission from ref. 222, Copyright 2020, Wiley-VCH.

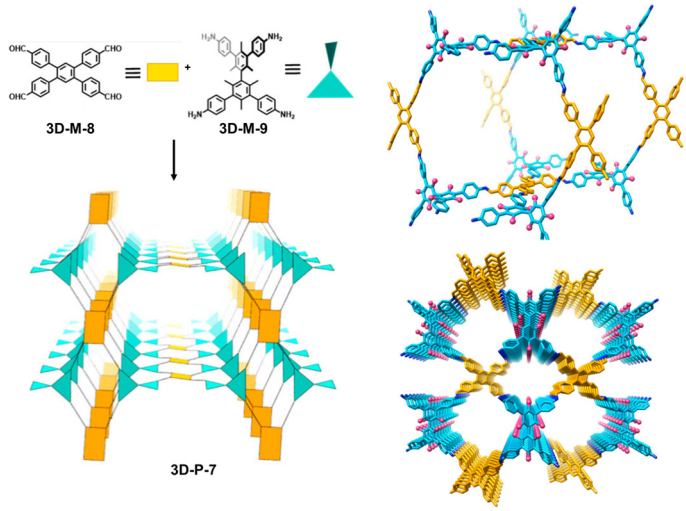

Fig. 27 Synthesis and the single-crystal structure of 3D-P-7. Reproduced with permission from ref. 223, Copyright 2020, American Chemical Society.

although the sizes are usually too small to be analyzed by SCXRD. cRED has emerged as a powerful alternative method for characterizing small single crystal structures.[15, 16] In 2013, Yaghi and co-workers reported a cRED technique for the structure determination of a 3D COF (**3D-P-8**) (Fig. 28).[16] After collecting the cRED data, the 3D reciprocal lattice was reconstructed with a resolution of up to 1.5 Å (Fig. 28b) and the structure of **3D-P-8** was successfully determined in the space group *I*$\bar{4}$2*d* (Fig. 28c).

Wang and Sun further explored such a method and employed 3D cRED technique to determine the structures.[14, 223, 224] They developed a novel topology design approach for constructing

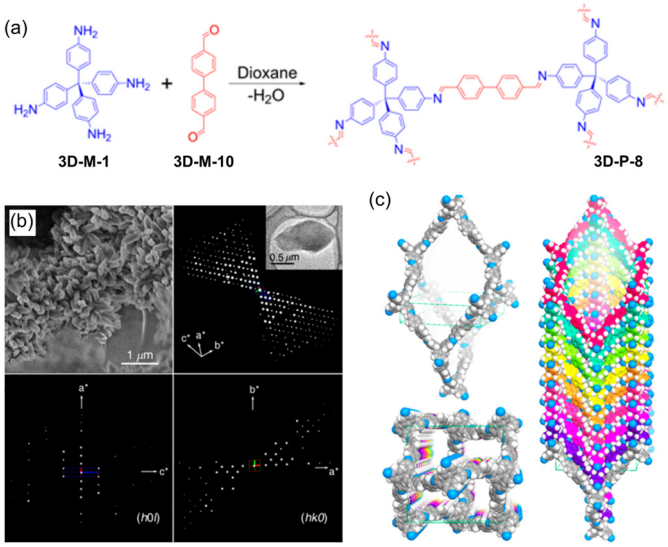

Fig. 28 The cRED technique for the structure determination of 3D COF: (a) Synthesis of **3D-P-8**. (b) Morphology and electron diffraction of **3D-P-8**. (c) Single-crystal structure of **3D-P-8.** Reproduced with permission from ref. 16, Copyright 2013, American Chemical Society.

3D COFs from tetrahedral or quadrilateral building blocks. Imine-linked 3D COF isostructures (**3D-P-9**, **3D-P-10**, and **3D-P-11**) were synthesized through a "4 + 4" reaction (Fig. 29a).[14] After optimization of the reaction conditions, single crystals with octahedral shape and size up to 1 μm were obtained (Fig. 29c). The 3D cRED technique proved capable of resolving the locations of the atoms except for H in the 3D structures of **3D-P-9**, **3D-P-10**, and **3D-P-11**, which show 5-fold interpenetrated pts nets with a resolution of 0.9 Å (Fig. 29b).

The development of the cRED technique allows us to explore the changes in topology through steric control. As shown in Fig. 30a and b, Wang and Sun synthesized three 3D COFs from similar precursors. The change in the substituents from methoxy groups to phenyl groups in the monomers changed the topology of the corresponding 3D COFs accordingly.[225] Two 3D COFs with totally different topologies were obtained. Based on cRED analysis, **3D-P-12** adopts a pts topology with a 5-fold interpenetrated structure, whereas **3D-P-13** was found to have a new ljh topology. When the substituents were changed to OH groups (**3D-P-14**), a reversible transformation was found in the switchable 3D COF through a quinone/hydroquinone redox reaction (Fig. 30c).[226]

As is widely recognized, rigid building blocks are typically used in synthesizing 3D COFs due to their preorganized structure, which can minimize system entropy loss and facilitate the formation of ordered structures. Although the concept of constructing 3D COFs with flexible linkers is appealing, there have been only few successful examples reported due to the challenges in the synthesis and structure characterization. Flexible framework structures have demonstrated intriguing characteristics such as reversible expansion/contraction upon vapor adsorption/desorption and distinctive breathing behavior, establishing them as a new type of soft porous crystals. Recently, Wang and Sun reported a 3D COF (**3D-P-15**) with flexible ether linkages in the backbone (Fig. 31a).[224] Despite achieving a resolution of approximately 1 Å, the direct determination of the structure of **3D-P-15** using cRED data was not possible due to the signal-to-noise ratio below 2 at high resolution (>1.5 Å) and a completeness of around 40%. They, therefore, implemented an advanced data procession method typically used in protein structure determination, involving the scaling and merging of 17 cRED data sets. This ultimately led to the successful establishment of a complete structure model of **3D-P-15**, adopting a pts topology with a 6-fold interpenetration (Fig. 31b) The flexibility of **3D-P-15** enabled by the flexible ether linkage allowed for a reversible expansion/contraction process upon vapor adsorption and desorption. However, the successful preparation of single crystal **3D-P-15** presented a significant challenge due to the free rotation of the C–O single bonds in the building block **3D-M-17**. Achieving success required a judicious combination of the flexible **3D-M-17** and the rigid **3D-M-1** building block and numerous trials to identify optimized reaction conditions contributed to the success.

Conventional solvothermal synthesis has yielded many successful examples of small-sized, single-crystalline 3D

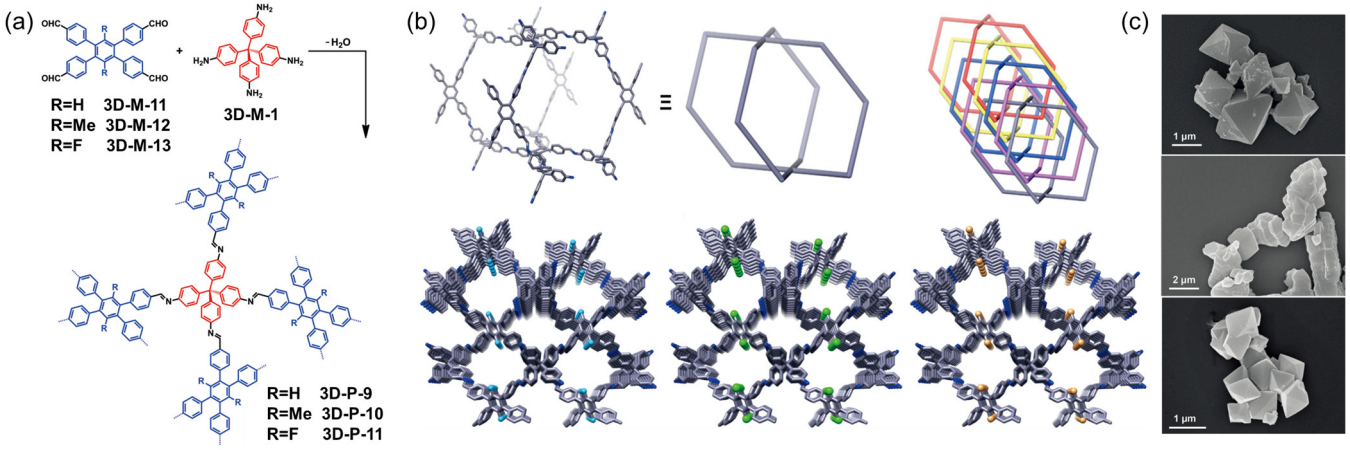

Fig. 29 The cRED technique for the structural determination of 3D COFs: (a) Synthesis of three 3D COFs (**3D-P-9**, **3D-P-10**, and **3D-P-11**); (b) Structural representations of **3D-P-9**, **3D-P-10**, and **3D-P-11**; (c) SEM images of **3D-P-9** (top), **3D-P-10** (middle), and **3D-P-11** (down). Reproduced with permission from ref. 14, Copyright 2019, Wiley-VCH.

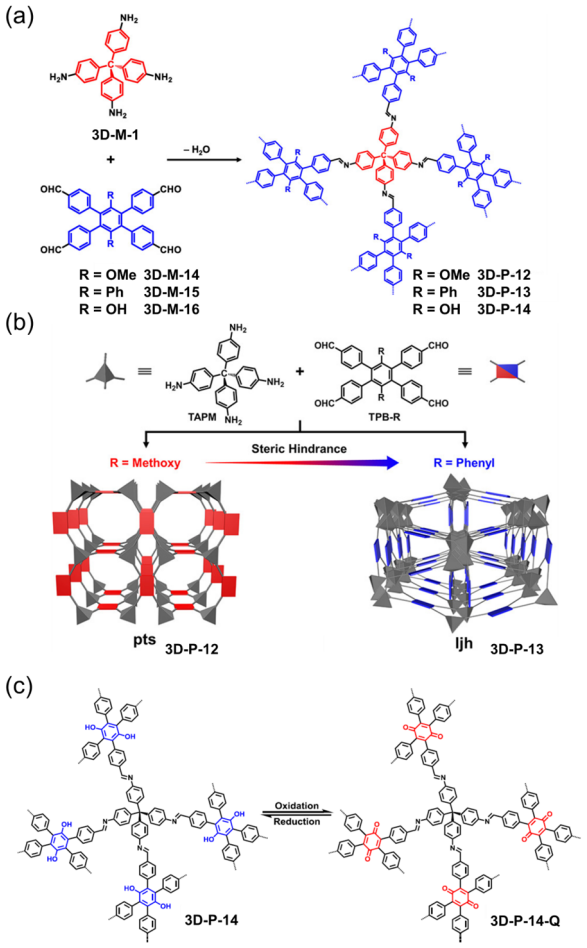

Fig. 30 Substituent effect on the topologies of 3D COFs: (a) Synthesis of **3D-P-12**, **3D-P-13**, **3D-P-14**; Reproduced with permission from ref. 225, Copyright 2021, American Chemical Society. (b) Tuning the topology of **3D-P-12** (pts) and **3D-P-13** (ljh) via steric control; (c) The oxidation and reduction process of **3D-P-14**. Reproduced with permission from ref. 226, Copyright 2020, Springer Nature.

COFs.[227, 228] Unlike the case for 2D COFs, the growth in 3D directions in solution appears to favor the formation of ordered structures, while interlayer slippage, common in 2D COFs, is detrimental to crystallization. Nonetheless, optimizing reaction conditions for the preparation of single-crystal 3D COFs typically requires costly and time-consuming trial-and-error experiments, with no proven effective guidelines yet identified. With the technological development of characterization, particularly the cRED technique and the emergence of commercial instruments, it is expected that more and more diverse single-crystal 3D COFs will emerge. Moreover, the development of new types of organic reactions beyond the Schiff-base reaction would be of great interest, given that current examples are all based on the formation of imine bonds.

3.1.3 Amphiphilic amino-acid assisted aqueous-phase synthesis

Recently, Zheng, Sun, Liu, and co-workers reported an amphiphilic-amino-acid-assisted strategy to prepare single-crystal imine-linked COFs in aqueous solutions under ambient conditions.[229] The amphiphilic amino-acid molecules can self-assemble into micelles and serve as dynamic barriers to prevent the precipitation of materials from the polymerization of the monomers in water, thus synthesizing single-crystal COFs (Fig. 32). This strategy shows good universality, and five types of 3D single-crystal COFs were obtained. **3D-M-1** is selected as the amine monomer, **3D-M-18**, **2D-M-3**, **3D-M-10**, and **3D-M-19** **3D-M-20** containing electron-accepting, electron-donating, and heterocyclic groups next to the aldehydes are chosen as the aldehyde-based monomers. Palmitoylglycine (C_{16}-GlyA) acts as the amphiphilic amino-acid and can assemble into micelles with a layered supramolecular structure in water, affording a hydrophobic compartment. The aldehyde-based monomer was first dissolved into the C_{16}-GlyA emulsion. The subsequent addition of *p*-toluenesulfonic acid-protonated **3D-M-1** led to gel-like mixtures, which are oligomers of polyimines. As the reaction proceeded, the disordered phase gradually transformed into crystals. Pure single-crystal COFs were obtained after a long-time reaction (14 days). The single-crystal structure of **3D-P-16** exhibits a diamond-type topology with seven-fold interpenetration. 1D straight channels along the interpenetration direction were observed. The removal of C_{16}-GlyA leads to a notable framework distortion. Similar to the case of **3D-P-16**, all non-hydrogen atoms of the **3D-P-2**, **3D-P-8**, **3D-P-17**, and **3D-P-18** crystals were identified. Notably, the single-crystal sizes of **3D-P-16** and **3D-P-18** are large enough for SCXRD analysis. The three left structures were resolved by the cRED technique.

3.1.4 Metal-coordinated synthesis

Besides the traditional 3D COFs, Yaghi and co-workers developed a single-crystal 3D woven structure made of helical threads. The term "weaving" was used to describe the interlacing of 1D units that make 2D and 3D structures.[230] Although these woven structures are made of 1D chains, the overall structures are 2D or 3D due to the metal-coordinated interaction to weave the 1D chains together.[230] A starting material with tetrahedral geometry, the phenanthroline-Cu complex containing four aldehyde groups (Fig. 33a), was chosen for the synthesis of a 3D COF via a Schiff base reaction with the linear linker benzidine. The resulting imine-linked threads were precisely brought together by copper ions, which act as templates, yielding a 3D framework with a weaving arrangement. Thanks to the tetrahedral geometry of the phenanthroline-Cu complex, the threads can be assembled into framework. The structure was resolved using 3D electron diffraction tomography (3D-EDT), which showed that **3D-P-19** has an orthorhombic Bravais lattice with a C-center. According to the refined model, **3D-P-19** crystallizes in a two-fold interpenetrated 3D framework with a dia topology. Notably, this material exhibits an unusual behavior in elasticity, likely because of its unique weaving structure. Subsequently, the same group used similar tetrahedral building units based on metal complexes to achieve a symmetrical arrangement of the organic threads to obtain a 3D woven structure with diamond topology (Fig. 33b).[231] The complex of cobalt and bis(diiminopyridine) acts as the tetrahedral building blocks with a dihedral angle of 80°. Unlike the previous study, the Boc-

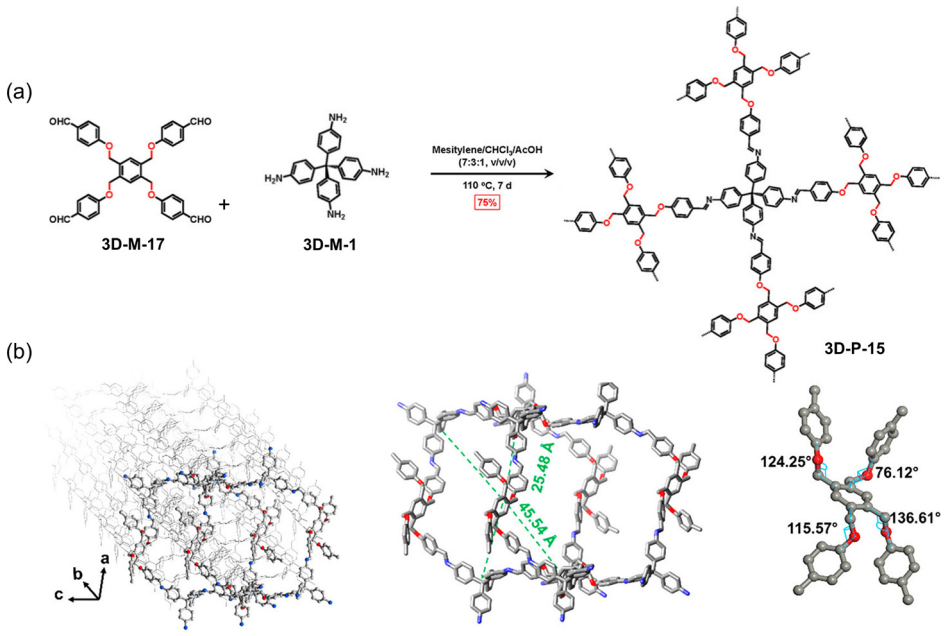

Fig. 31 An example of flexible 3D COF: (a) Synthesis of **3D-P-15**; (b) The single-crystal structure and the interpenetration of **3D-P-15**. Reproduced with permission from ref. 224, Copyright 2021, American Chemical Society.

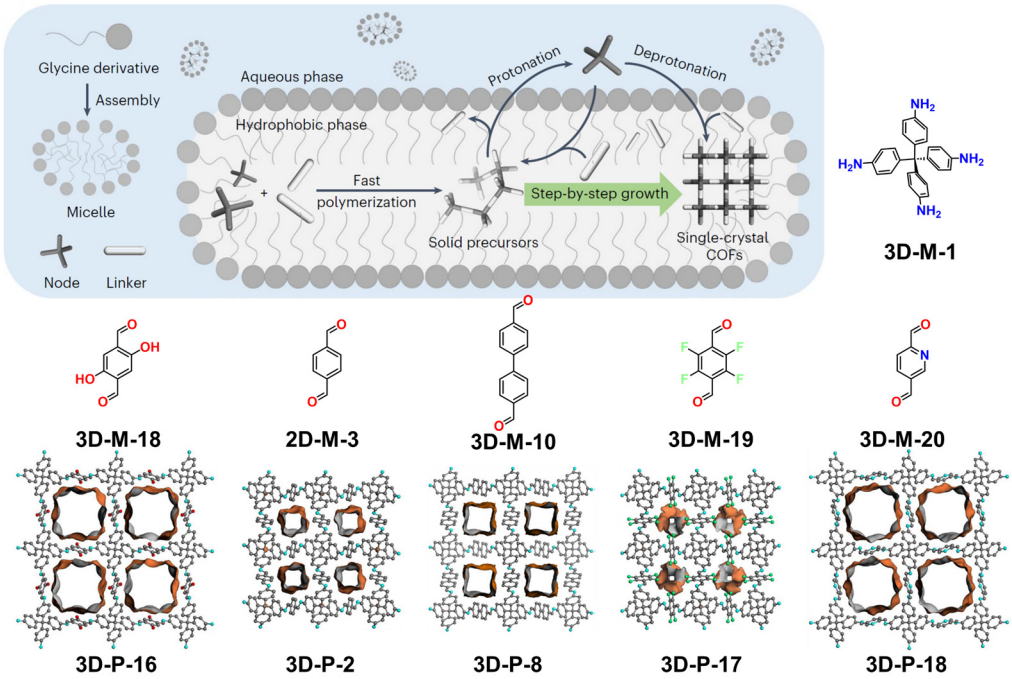

Fig. 32 Schematic diagram of the amphiphilic amino-acid-assisted aqueous-phase synthesis; chemical structures of monomer and single crystal structures of the prepared 3D COFs. Reproduced with permission from ref. 229, Copyright 2023, Springer Nature.

protected amine was used as the starting material, which was gradually deprotected to slow down the imine condensation reaction and facilitate the crystallization process. The structure of **3D-P-20** was solved by electron crystallography and X-ray analysis, showing **3D-P-20** has a very simple 3D woven structure. Only two sets of straight and parallel threads were observed in the structure to form one point of the registry.

Based on the previous work of **3D-P-20**, Yaghi and co-workers further reported a new isoreticular woven metallated **3D-P-21** (Fig. 33c).[232] In this work, the BF_4^- counter anions were exchanged with $PO_2Ph_2^-$ anions to fill the internal voids of the COFs. Thus, the interpenetration during the framework formation was successfully prevented in the case of **3D-P-21**. 3D-EDT revealed a monoclinic Bravais lattice of **3D-P-21**. The experimental PXRD pattern and HRTEM showed that **3D-P-21** belongs to the monoclinic space group *Pc*. Notably, **3D-P-21**, which contains a 3D pore system with a large channel, exhibits adaptive dynamics for vapor and dye inclusion.

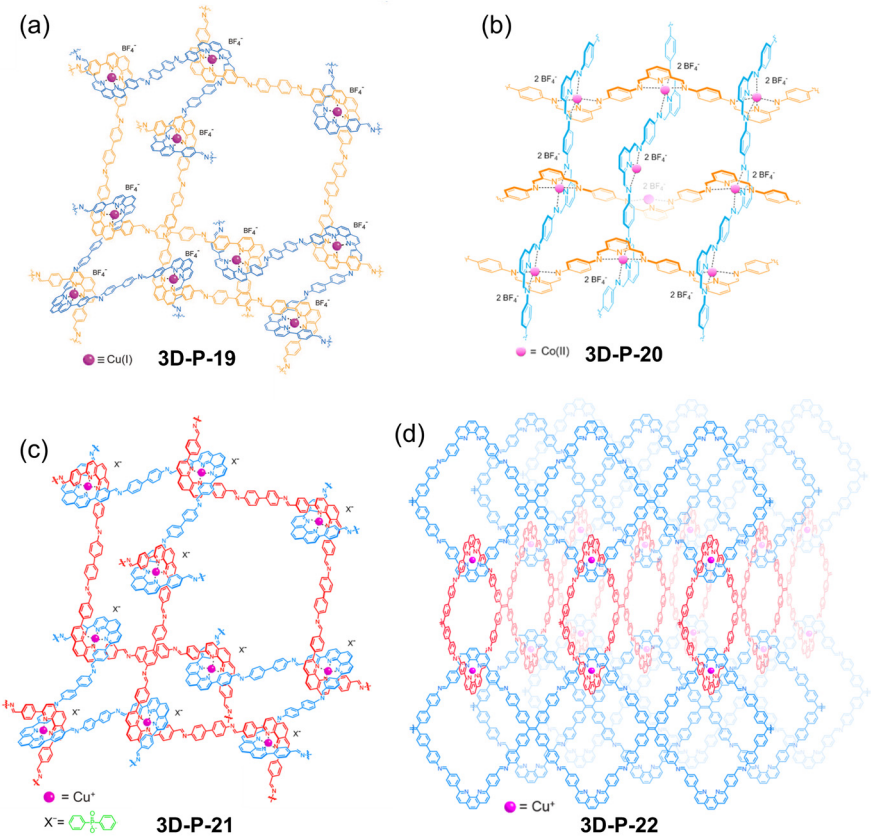

Fig. 33 Chemical structures of four examples of 3D woven COFs: (a) **3D-P-19**. Reproduced with permission from ref. 230, Copyright 2016, American Association for the Advancement of Science. (b) **3D-P-20**. Reproduced with permission from ref. 231, Copyright 2017, American Chemical Society. (c) **3D-P-21**. Reproduced with permission from ref. 232, Copyright 2018, American Chemical Society. (d) **3D-P-22**. Reproduced with permission from ref. 233, Copyright 2019, American Chemical Society.

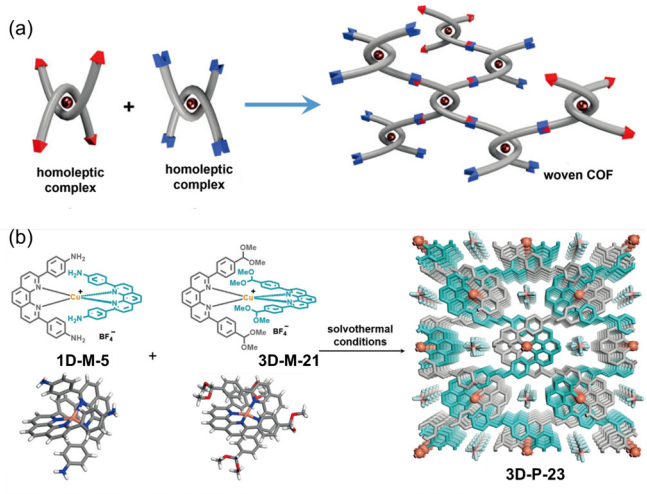

Fig. 34 3D woven COF: (a) The strategy of constructing 3D woven COF (**3D-P-23**); (b) The synthesis and the crystal structure of **3D-P-23**. Reproduced with permission from ref. 63, Copyright 2023, Springer Nature.

In a recent study, Yaghi and co-workers developed a new extended 3D COF structure with mechanical entanglement.[233] The framework was created by interlocking 1D ribbons of corner-sharing squares constituted entirely of covalently linked organic molecules (Fig. 33d). Similar to their previous work, they used the copper(I)-bisphenanthroline complex salt as the tetrahedral tetratopic units. However, instead of a linear ditopic benzidine linker, the square-planar tetratopic units were used to construct an extended 3D COF (**3D-P-22**) through interlocking of 1D corner-sharing square ribbons. The structure of **3D-P-22** with pts topology was revealed by electron microscopy and X-ray powder diffraction.

Loh and co-workers reported a 3D woven COF (**3D-P-23**), which was synthesized via the reaction between two stable metal complexes **1D-M-5** and **3D-M-21** (Fig. 34).[63] The structure of the 3D woven COF was characterized by 3D ED and PXRD. **3D-P-23** exhibits a dia topology with a three-fold interpenetrated structure. Cu ions in the tetrahedral building units serve as a node to organize the interlacing of the threads.

Crystalline woven materials are a valuable addition to the field of reticular chemistry, enriching the library of materials. It is possible to grow single crystals of these woven COFs. The presence of the metal may facilitate their crystallization. The structures of 3D woven COFs could be elucidated through a combination of techniques, including the electron diffraction technique, PXRD, and HRTEM.

3.1.5 Exploration of new linkages

The majority of single-crystal 3D COFs that have been reported in the literature are based on Schiff base chemistry and are synthesized by polycondensation of aldehydes and amines. The dynamic self-adjusting process is critical for achieving the thermodynamic equilibrium and ultimately forming highly

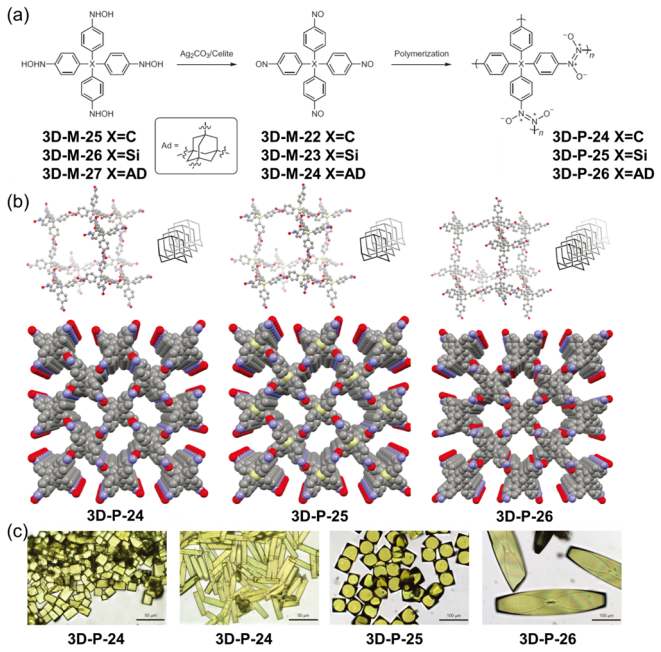

Fig. 35 Diamondoid azodioxy 3D SCPs: (a) Synthesis of three covalent organic networks **3D-P-24, 3D-P-25**, and **3D-P-26** by reversible self-addition polymerizations; (b) Single-crystal structures of **3D-P-24, 3D-P-25**, and **3D-P-26**; (c) Optical microscopy images of the single crystals **3D-P-24, 3D-P-25**, and **3D-P-26**. Reproduced with permission from ref. 10, Copyright 2013, Springer Nature.

ordered structures. However, exploring new reaction pathways for preparing single-crystal 3D COFs with new linkages beyond the imine bond is highly encouraged and attractive. Despite numerous attempts to synthesize 3D COFs using novel linkages, successful examples of non-imine-bonded single-crystal 3D COFs with an unambiguous structure elucidation are very rare. In 2013, Wuest and co-workers reported several examples of single crystals of 3D covalent organic networks (**3D-P-24**, **3D-P-25**, **3D-P-26**).[10] The reversible self-addition polymerization of nitroso was utilized to realize the error-correction process. The authors found that the azodioxy linkers are suitable for the construction of single-crystal covalent organic networks due to their good reversibility, which is the key to this strategy. Three different monomers with nitrous groups all converted to the corresponding diamondoid azodioxy networks as single crystals, which were characterized by SCXRD (Fig. 35a, b, and c).

3.2 Topochemical polymerization

Unlike the topochemical approach used for the preparation of 2D SCPs, successful examples of 3D SCPs preparation are extremely rare. Ke and co-workers reported one successful example (**3D-P-1**), which was discussed in section 2.2 (Fig. 19) together with the **2D-P-9** with a 2D structure for the sake of organizational coherence. The design concept and synthetic strategy for 3D SCPs are similar to those of the 2D SCPs discussed in section 2.2. While there are certainly challenges to overcome, as is also the case with the preparation of 2D SCPs, the current scarcity of successful examples is both intriguing and motivating for researchers to continue exploring this field. For example, Dincă and co-workers recently reported the preparation of crystalline 3D porous organic polymer with C–C

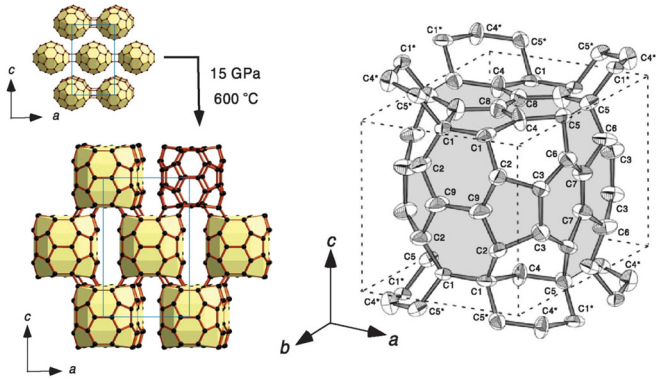

Fig. 36 Single-crystal structure of the 3D C60 SPC **3D-P-27**. Reproduced with permission from ref. 208, Copyright 2023, American Physical Society.

bond linkages by using topochemical polymerization. Photoactive anthracene derivatives were connected to a tetraphenylmethane core to form the single-crystal monomer.[234] Although the transformation from monomer to polymer through [4+4] photo-dimerization between the anthracene preserved crystallinity, efforts to obtain single crystals of the polymer were unsuccessful due to the large displacement of monomer molecules during the photopolymerization. While efforts to obtain single crystals of 3D polymers through [4+4] photo-dimerization have been unsuccessful. It is important to note that significant progress has been achieved, and the researchers were on the brink of success. Furthermore, the achievements in the field of 2D SCPs preparation through topochemical polymerization provide a solid foundation for the belief that rational monomer design and continued exploration will lead to the realization of 3D SCPs with promising properties.

3.3 Others

In addition to the traditional synthetic strategies, high-pressure synthesis offers an alternative method for preparing single-crystal samples of 3D architectures,[208] as demonstrated by Yamanaka and co-workers in their work on 2D C_{60} SCP (discussed in section 2.3).[206, 209] In 2006, they were able to convert the 2D C_{60} SCPs into 3D C_{60} SCPs (Fig. 36) using high pressure and temperature (15 GPa and 600 °C).[208]. The conversion occurred topochemically, preserving the basic structure of the individual 2D structure. The resulting single-crystal structure of **3D-P-27** revealed that each C_{60} unit was deformed into a cuboid-shaped rectangular parallelepiped and linked to 8 cuboid neighbors in the body-centered cell by [3+3] cycloaddition. Unlike the nonconductive 2D C_{60} polymer, **3D-P-27** is electron conductive. The success of synthesizing 3D SCPs under high-pressure conditions is a promising development, which opens up possibilities for the synthesis of other 3D SCPs using similar methods. Further research in this area is highly recommended to explore these possibilities.

Conclusions

The study of SCPs has emerged as a highly popular research subject over the past decade. The synthesis of such SCPs

presents a challenging task for chemists, as they must exert complete control over the formation of chemical bonds as opposed to random polymerization. An atomic-level determination of atom positions, bond connections, and secondary interactions through single-crystal structure analysis can potentially offer solutions to many long-standing questions and concerns in polymeric architectures, including understanding polymerization mechanisms, controlling factors of structural orders, exploring potential applications based on their structures, and studying the physical properties of polymers.

Despite the potential benefits, the lack of general strategies to grow high-quality single crystals remains a significant challenge in SCPs synthesis. To date, solution synthesis and topochemical polymerization have been the primary strategies employed for the formation of SCPs. Although these methods offer great potential for the development of efficient and versatile SCP synthesis methods, both of these methods have limitations in terms of the choice of reaction types, and highly time-consuming trial-and-error experiments are unavoidable. Solution synthesis is highly dependent on imine-bond reactions, while topochemical polymerization is limited to irradiation- or heating-triggered reactions. Solution synthesis has the advantage of extending the topologies of the obtained structures, as the design of diversified monomers for structural diversity is much easier in this method. The polymerization kinetics are deemed to be critical based on the current understanding of solution synthesis. In contrast, topochemical polymerization is advantageous for the preparation of large-sized single crystals, as the size of the single-crystal monomers determines the size of the SCPs. Further studies in this area are highly encouraged to develop more efficient and versatile methods for the synthesis of SCPs.

The structure determination of the obtained SCPs at an atomic level is still limited to SCXRD and cRED. The cRED technique has become a well-accepted characterization technique for the structure determination of SCPs and will continue to play a key role in SCPs materials. The cRED technique, although demanding in terms of technical expertise and optimization of operating conditions, requires smaller single crystals compared to SCXRD. However, it has not gained as much popularity as SCXRD for structure determination due to its technical demands. Moreover, successful applications of cRED to 2D SCPs are scarce, underscoring the importance of the further investigation. Additionally, since both SCXRD and cRED demand high-quality single crystals, alternative techniques are needed to determine the crystal structures of polycrystalline samples and circumvent the need for growing large single crystals. Any advancements in instrumentation and characterization techniques should be leveraged for the structure determination of SCPs. Cross-disciplinary approaches, such as cryo-transmission electron microscopy (cryo-TEM), are also encouraged to overcome existing limitations.

Advancements in the development of strategies to obtain SCPs are expected to significantly improve the structural diversity of SCPs, particularly 2D and 3D SCPs, realizing their full potential in the near future. These SCPs possess highly ordered structures, well-defined pores, and channels that offer unique characteristics, making them ideal for precise separation technology, nano-confinement catalysis, organic single-crystal device, and many other applications. With an atomic-level determination of atom positions, bond connections, and secondary interactions through single-crystal structure analysis, researchers can gain insight into the structure-property relationship of these materials and reveal their intrinsic properties. Even though the application of SCPs has not been extensively studied, their immense potential is clear, and further research in this area is highly encouraged.

Author Contributions

Y.Z and W.Z initiated the concept. M.W, Y.J, W.Z and Y.Z wrote the review together.

Conflicts of interest

There are no conflicts to declare.

Acknowledgments

This work was supported by the National Natural Science Foundation of China (22175101), the Natural Science Foundation of Shandong Province (ZR2020ZD38), and the National Science Foundation (CHE-2108197).

Notes and references

1. H. Staudinger, *Ber. Dtsch. Chem. Ges.*, 1920, **53**, 1073-1085.
2. H. Staudinger and J. Fritschi, *Helv. Chim. Acta*, 1922, **5**, 785-806.
3. K. S. Novoselov, A. K. Geim, S. V. Morozov, D. Jiang, Y. Zhang, S. V. Dubonos, I. V. Grigorieva and A. A. Firsov, *Science*, 2004, **306**, 666-669.
4. P. Côté Adrien, I. Benin Annabelle, W. Ockwig Nathan, M. O'Keeffe, J. Matzger Adam and M. Yaghi Omar, *Science*, 2005, **310**, 1166-1170.
5. M. El-Kaderi Hani, R. Hunt Joseph, L. Mendoza-Cortés José, P. Côté Adrien, E. Taylor Robert, M. O'Keeffe and M. Yaghi Omar, *Science*, 2007, **316**, 268-272.
6. S. Diercks Christian and M. Yaghi Omar, *Science*, 2017, **355**, eaal1585.
7. M. Xue, J. Yang, F. Kang, X. Wang and Q. Zhang, *J. Mater. Chem. C*, 2022, **10**, 17027-17047.
8. B. Gui, H. Ding, Y. Cheng, A. Mal and C. Wang, *Trends Chem.*, 2022, **4**, 437-450.
9. M. J. Kory, M. Wörle, T. Weber, P. Payamyar, S. W. van de Poll, J. Dshemuchadse, N. Trapp and A. D. Schlüter, *Nat. Chem.*, 2014, **6**, 779-784.
10. D. Beaudoin, T. Maris and J. D. Wuest, *Nat. Chem.*, 2013, **5**, 830-834.
11. T. Ma, A. Kapustin Eugene, X. Yin Shawn, L. Liang, Z. Zhou, J. Niu, L.-H. Li, Y. Wang, J. Su, J. Li, X. Wang, D. Wang Wei, W. Wang, J. Sun and M. Yaghi Omar, *Science*, 2018, **361**, 48-52.
12. B. Gui, G. Lin, H. Ding, C. Gao, A. Mal and C. Wang, *Acc. Chem. Res.*, 2020, **53**, 2225-2234.

13. X. Guan, F. Chen, Q. Fang and S. Qiu, *Chem. Soc. Rev.*, 2020, **49**, 1357-1384.
14. C. Gao, J. Li, S. Yin, G. Lin, T. Ma, Y. Meng, J. Sun and C. Wang, *Angew. Chem. Int. Ed.*, 2019, **58**, 9770-9775.
15. W. Wan, J. Sun, J. Su, S. Hovmöller and X. Zou, *J. Appl. Crystallogr.*, 2013, **46**, 1863-1873.
16. Y.-B. Zhang, J. Su, H. Furukawa, Y. Yun, F. Gándara, A. Duong, X. Zou and O. M. Yaghi, *J. Am. Chem. Soc.*, 2013, **135**, 16336-16339.
17. P. H. Geil, *J. Polym. Sci.*, 1960, **44**, 449-458.
18. A. Keller, *Polymer*, 1962, **3**, 393-421.
19. A. Keller, *Kolloid Z. Z. Polym.*, 1969, **231**, 386-421.
20. E. Martuscelli, *J. Macromol. Sci., Part B*, 1975, **11**, 1-20.
21. R. H. Baughman, *J Polym Sci B Polym Phys Ed*, 1974, **12**, 1511-1535.
22. T. Okihara, M. Tsuji, A. Kawaguchi, K.-I. Katayama, H. Tsuji, S.-H. Hyon and Y. Ikada, *J. Macromol. Sci., Part B*, 1991, **30**, 119-140.
23. D. H. Kim, J. T. Han, Y. D. Park, Y. Jang, J. H. Cho, M. Hwang and K. Cho, *Adv. Mater.*, 2006, **18**, 719-723.
24. S. Z. D. Cheng, *Nature*, 2007, **448**, 1006-1007.
25. H. Li and L. A. Estroff, *Adv. Mater.*, 2009, **21**, 470-473.
26. L. Cartier, T. Okihara and B. Lotz, *Macromol.*, 1997, **30**, 6313-6322.
27. X. Liu, Y. Zhang, K. Goswami Dipak, S. Okasinski John, K. Salaita, P. Sun, J. Bedzyk Michael and A. Mirkin Chad, *Science*, 2005, **307**, 1763-1766.
28. C. H. M. Weber, A. Chiche, G. Krausch, S. Rosenfeldt, M. Ballauff, L. Harnau, I. Göttker-Schnetmann, Q. Tong and S. Mecking, *Nano Lett.*, 2007, **7**, 2024-2029.
29. B. Lotz, T. Miyoshi and S. Z. D. Cheng, *Macromol.*, 2017, **50**, 5995-6025.
30. W. A. Henderson, N. R. Brooks and V. G. Young, *J. Am. Chem. Soc.*, 2003, **125**, 12098-12099.
31. C. Zhang, S. Gamble, D. Ainsworth, A. M. Z. Slawin, Y. G. Andreev and P. G. Bruce, *Nat. Mater.*, 2009, **8**, 580-584.
32. A. J. Greenlee, C. I. Wendell, M. M. Cencer, S. D. Laffoon and J. S. Moore, *Trends Chem.*, 2020, **2**, 1043-1051.
33. A. Wilson, G. Gasparini and S. Matile, *Chem. Soc. Rev.*, 2014, **43**, 1948-1962.
34. D. Wang, L. Zhang and Y. Zhao, *J. Org. Chem.*, 2022, **87**, 2767-2772.
35. M. Mastalerz, *Angew. Chem. Int. Ed.*, 2010, **49**, 5042-5053.
36. Y. Jin, C. Yu, R. J. Denman and W. Zhang, *Chem. Soc. Rev.*, 2013, **42**, 6634-6654.
37. Y. Jin, Q. Wang, P. Taynton and W. Zhang, *Acc. Chem. Res.*, 2014, **47**, 1575-1586.
38. M. E. Belowich and J. F. Stoddart, *Chem. Soc. Rev.*, 2012, **41**, 2003-2024.
39. A. G. Orrillo and R. L. E. Furlan, *Angew. Chem. Int. Ed.*, 2022, **61**, e202201168.
40. F. Schaufelberger, B. J. J. Timmer and O. Ramström, in *Dynamic Covalent Chemistry*, 2017, DOI: 10.1002/9781119075738.ch1, pp. 1-30.
41. T. Hasell and A. I. Cooper, *Nat. Rev. Mater.*, 2016, **1**, 16053.
42. W. Zhang and Y. Jin, 2017.
43. S. Huang, Z. Lei, Y. Jin and W. Zhang, *Chem. Sci.*, 2021, **12**, 9591-9606.
44. X. Li, P. Yadav and K. P. Loh, *Chem. Soc. Rev.*, 2020, **49**, 4835-4866.
45. R. R. Liang, S. Y. Jiang, A. Ru-Han and X. Zhao, *Chem. Soc. Rev.*, 2020, **49**, 3920-3951.
46. Y. H. Jin, Y. M. Hu and W. Zhang, *Nat. Rev. Chem.*, 2017, **1**.
47. P. J. Waller, F. Gandara and O. M. Yaghi, *Acc. Chem. Res.*, 2015, **48**, 3053-3063.
48. K. Y. Geng, T. He, R. Y. Liu, S. Dalapati, K. T. Tan, Z. P. Li, S. S. Tao, Y. F. Gong, Q. H. Jiang and D. L. Jiang, *Chem. Rev.*, 2020, **120**, 8814-8933.
49. S. Y. Ding and W. Wang, *Chem. Soc. Rev.*, 2013, **42**, 548-568.
50. Y. S. Li, W. B. Chen, G. L. Xing, D. L. Jiang and L. Chen, *Chem. Soc. Rev.*, 2020, **49**, 2852-2868.
51. R. Y. Liu, K. T. Tan, Y. F. Gong, Y. Z. Chen, Z. E. Li, S. L. Xie, T. He, Z. Lu, H. Yang and D. L. Jiang, *Chem. Soc. Rev.*, 2021, **50**, 120-242.
52. J. L. Segura, M. J. Mancheno and F. Zamora, *Chem. Soc. Rev.*, 2016, **45**, 5635-5671.
53. J. C. Jiang, Y. B. Zhao and O. M. Yaghi, *J. Am. Chem. Soc.*, 2016, **138**, 3255-3265.
54. S. Kandambeth, K. Dey and R. Banerjee, *J. Am. Chem. Soc.*, 2019, **141**, 1807-1822.
55. N. Huang, P. Wang and D. L. Jiang, *Nat. Rev. Mater.*, 2016, **1**.
56. H.-S. Xu, Y. Luo, X. Li, P. Z. See, Z. Chen, T. Ma, L. Liang, K. Leng, I. Abdelwahab, L. Wang, R. Li, X. Shi, Y. Zhou, X. F. Lu, X. Zhao, C. Liu, J. Sun and K. P. Loh, *Nat. Commun.*, 2020, **11**, 1434.
57. A. R. Navarro Jorge, *Science*, 2018, **361**, 35-35.
58. Y. Hu, S. J. Teat, W. Gong, Z. Zhou, Y. Jin, H. Chen, J. Wu, Y. Cui, T. Jiang, X. Cheng and W. Zhang, *Nat. Chem.*, 2021, **13**, 660-665.
59. J. Atcher, P. Mateus, B. Kauffmann, F. Rosu, V. Maurizot and I. Huc, *Angew. Chem. Int. Ed.*, 2021, **60**, 2574-2577.
60. S. De, B. Chi, T. Granier, T. Qi, V. Maurizot and I. Huc, *Nat. Chem.*, 2018, **10**, 51-57.
61. Q. Gan, Y. Ferrand, C. Bao, B. Kauffmann, A. Grélard, H. Jiang and I. Huc, *Science*, 2011, **331**, 1172-1175.
62. J. L. Greenfield, F. J. Rizzuto, I. Goldberga and J. R. Nitschke, *Angew. Chem. Int. Ed.*, 2017, **56**, 7541-7545.
63. H.-S. Xu, Y. Luo, P. Z. See, X. Li, Z. Chen, Y. Zhou, X. Zhao, K. Leng, I.-H. Park, R. Li, C. Liu, F. Chen, S. Xi, J. Sun and K. P. Loh, *Angew. Chem. Int. Ed.*, 2020, **59**, 11527-11532.
64. K. Tanaka and F. Toda, *Chem. Rev.*, 2000, **100**, 1025-1074.
65. K. Biradha and R. Santra, *Chem. Soc. Rev.*, 2013, **42**, 950-967.
66. X. Xiao, H. Wang, P. Urbankowski and Y. Gogotsi, *Chem. Soc. Rev.*, 2018, **47**, 8744-8765.
67. K. Hema, A. Ravi, C. Raju, J. R. Pathan, R. Rai and K. M. Sureshan, *Chem. Soc. Rev.*, 2021, **50**, 4062-4099.
68. K. Hema and K. M. Sureshan, *Acc. Chem. Res.*, 2019, **52**, 3149-3163.
69. J. W. Lauher, F. W. Fowler and N. S. Goroff, *Acc. Chem. Res.*, 2008, **41**, 1215-1229.
70. S.-L. Huang, T. S. A. Hor and G.-X. Jin, *Coord. Chem. Rev.*, 2017, **346**, 112-122.
71. T. Friščić and L. R. MacGillivray, *Z Med Phys*, 2005, **220**, 351-363.
72. T. Devic, P. Batail and N. Avarvari, *Chem. Commun.*, 2004, DOI: 10.1039/B404482G, 1538-1539.
73. S. P. Yelgaonkar, G. Campillo-Alvarado and L. R. MacGillivray, *J. Am. Chem. Soc.*, 2020, **142**, 20772-20777.
74. Q. Chu, D. C. Swenson and L. R. MacGillivray, *Angew. Chem. Int. Ed.*, 2005, **44**, 3569-3572.
75. M. Garai, R. Santra and K. Biradha, *Angew. Chem. Int. Ed.*, 2013, **52**, 5548-5551.

76. H. A. Al-Mohsin, A. AlMousa, S. A. Oladepo, A. S. Jalilov, M. Fettouhi and A. M. P. Peedikakkal, *Inorg. Chem.*, 2019, **58**, 10167-10173.
77. Q.-H. Guo, M. Jia, Z. Liu, Y. Qiu, H. Chen, D. Shen, X. Zhang, Q. Tu, M. R. Ryder, H. Chen, P. Li, Y. Xu, P. Li, Z. Chen, G. S. Shekhawat, V. P. Dravid, R. Q. Snurr, D. Philp, A. C. H. Sue, O. K. Farha, M. Rolandi and J. F. Stoddart, *J. Am. Chem. Soc.*, 2020, **142**, 6180-6187.
78. Q. Yu, M. Li, J. Gao, P. Xu, Q. Chen, D. Xing, J. Yan, M. J. Zaworotko, J. Xu, Y. Chen, P. Cheng and Z. Zhang, *Angew. Chem. Int. Ed.*, 2019, **58**, 18634-18640.
79. M. Servalli, N. Trapp and A. D. Schlüter, *Chem. - Eur. J.*, 2018, **24**, 15003-15012.
80. P. Kissel, D. J. Murray, W. J. Wulftange, V. J. Catalano and B. T. King, *Nat. Chem.*, 2014, **6**, 774-778.
81. I. Turowska-Tyrk and E. Trzop, *Acta Crystallogr. Sect. B*, 2003, **59**, 779-786.
82. A. Matsumoto, T. Tanaka, T. Tsubouchi, K. Tashiro, S. Saragai and S. Nakamoto, *J. Am. Chem. Soc.*, 2002, **124**, 8891-8902.
83. T. Tanaka and A. Matsumoto, *J. Am. Chem. Soc.*, 2002, **124**, 9676-9677.
84. R. Samanta, D. Kitagawa, A. Mondal, M. Bhattacharya, M. Annadhasan, S. Mondal, R. Chandrasekar, S. Kobatake and C. M. Reddy, *ACS Applied Materials & Interfaces*, 2020, **12**, 16856-16863.
85. C. L. Anderson, H. Li, C. G. Jones, S. J. Teat, N. S. Settineri, E. A. Dailing, J. Liang, H. Mao, C. Yang, L. M. Klivansky, X. Li, J. A. Reimer, H. M. Nelson and Y. Liu, *Nat. Commun.*, 2021, **12**, 6818.
86. T. Itoh, S. Nomura, H. Nakasho, T. Uno, M. Kubo, N. Tohnai and M. Miyata, *Macromol.*, 2015, **48**, 5450-5455.
87. T.-J. Hsu, F. W. Fowler and J. W. Lauher, *J. Am. Chem. Soc.*, 2012, **134**, 142-145.
88. J. J. Kane, R.-F. Liao, J. W. Lauher and F. W. Fowler, *J. Am. Chem. Soc.*, 1995, **117**, 12003-12004.
89. P. Baillargeon, R. Robidas, C. Y. Legault, T. Rahem, A. Paré Fouapon and S.-M. Boivin, *Cryst. Growth Des.*, 2020, **20**, 5648-5656.
90. J. Xiao, M. Yang, J. W. Lauher and F. W. Fowler, *Angew. Chem. Int. Ed.*, 2000, **39**, 2132-2135.
91. A. Sun, W. Lauher Joseph and S. Goroff Nancy, *Science*, 2006, **312**, 1030-1034.
92. G. Wegner, *Makromol. Chem.*, 1972, **154**, 35-48.
93. V. Athiyarath and K. M. Sureshan, *Angew. Chem. Int. Ed.*, 2020, **59**, 15580-15585.
94. K. Hema and K. M. Sureshan, *Angew. Chem. Int. Ed.*, 2019, **58**, 2754-2759.
95. A. Pathigoolla and K. M. Sureshan, *Angew. Chem. Int. Ed.*, 2013, **52**, 8671-8675.
96. A. Pathigoolla and K. M. Sureshan, *Angew. Chem. Int. Ed.*, 2014, **53**, 9522-9525.
97. R. Mohanrao and K. M. Sureshan, *Angew. Chem. Int. Ed.*, 2018, **57**, 12435-12439.
98. V. Athiyarath and K. M. Sureshan, *Angew. Chem. Int. Ed.*, 2019, **58**, 612-617.
99. V. Athiyarath, M. C. Madhusudhanan, S. Kunnikuruvan and K. M. Sureshan, *Angew. Chem. Int. Ed.*, 2022, **61**, e202113129.
100. W.-W. He, S.-L. Li and Y.-Q. Lan, *Inorg. Chem. Front.*, 2018, **5**, 279-300.
101. A. Chaudhary, A. Mohammad and S. M. Mobin, *Cryst. Growth Des.*, 2017, **17**, 2893-2910.
102. F. Hu, X. Bi, X. Chen, Q. Pan and Y. Zhao, *Chem. Lett.*, 2021, **50**, 1015-1029.
103. M. Hasegawa, Y. Suzuki, F. Suzuki and H. Nakanishi, *J. Polym. Sci., Part A-1: Polym. Chem.*, 1969, **7**, 743-752.
104. V. Buchholz and V. Enkelmann, *Mol. Cryst. Liq. Cryst. Sci. Technol., Sect. A*, 2001, **356**, 315-325.
105. K. Tashiro, H. Yamamoto, K. Sugimoto, T. Takahama, M. Tanaka and M. Hasegawa, *Macromol.*, 2019, **52**, 2189-2202.
106. G. W. Coates, A. R. Dunn, L. M. Henling, J. W. Ziller, E. B. Lobkovsky and R. H. Grubbs, *J. Am. Chem. Soc.*, 1998, **120**, 3641-3649.
107. R. Mandal, M. Garai and K. Biradha, *Cryst. Growth Des.*, 2017, **17**, 5061-5064.
108. R. Mandal, A. Garai, S. Peli, P. K. Datta and K. Biradha, *Chem. - Eur. J.*, 2020, **26**, 396-400.
109. P. Johnston, C. Braybrook and K. Saito, *Chem. Sci.*, 2012, **3**, 2301-2306.
110. P. Johnston, D. Wheldale, C. Braybrook and K. Saito, *Polym. Chem.*, 2014, **5**, 4375-4384.
111. Z. Wang, B. Kastern, K. Randazzo, A. Ugrinov, J. Butz, D. W. Seals, M. P. Sibi and Q. R. Chu, *Green Chem.*, 2015, **17**, 4720-4724.
112. Z. Wang, B. Miller, J. Butz, K. Randazzo, Z. D. Wang and Q. R. Chu, *Angew. Chem. Int. Ed.*, 2017, **56**, 12155-12159.
113. Y. Liu, X.-R. Guan, D.-C. Wang, J. F. Stoddart and Q.-H. Guo, *J. Am. Chem. Soc.*, 2023, **145**, 13223-13231.
114. S. Saragai, K. Tashiro, S. Nakamoto, T. Kamae, A. Matsumoto and T. Tsubouchi, *Polym. J.*, 2001, **33**, 199-203.
115. A. Matsumoto, T. Odani, M. Chikada, K. Sada and M. Miyata, *J. Am. Chem. Soc.*, 1999, **121**, 11122-11129.
116. A. Matsumoto, T. Kunisue, S. Nagahama, A. Matsumoto, K. Sada, K. Inoue, T. Tanakaand and M. Miyata, *Mol. Cryst. Liq. Cryst.*, 2003, **390**, 11-18.
117. S. Nagahama and A. Matsumoto, *J. Am. Chem. Soc.*, 2001, **123**, 12176-12181.
118. T. Odani, S. Okada, C. Kabuto, T. Kimura, S. Shimada, H. Matsuda, H. Oikawa, A. Matsumoto and H. Nakanishi, *Cryst. Growth Des.*, 2009, **9**, 3481-3487.
119. A. Matsumoto, D. Furukawa and H. Nakazawa, *J. Polym. Sci., Part A: Polym. Chem.*, 2006, **44**, 4952-4965.
120. A. Matsumoto, T. Tanaka and K. Oka, *Synthesis*, 2005, **2005**, 1479-1490.
121. A. Matsumoto, D. Furukawa, Y. Mori, T. Tanaka and K. Oka, *Cryst. Growth Des.*, 2007, **7**, 1078-1085.
122. Y. Mori, T. Chiba, T. Odani and A. Matsumoto, *Cryst. Growth Des.*, 2007, **7**, 1356-1364.
123. X. Hou, Z. Wang, J. Lee, E. Wysocki, C. Oian, J. Schlak and Q. R. Chu, *Chem. Commun.*, 2014, **50**, 1218-1220.
124. Y. Mori and A. Matsumoto, *Cryst. Growth Des.*, 2007, **7**, 377-385.
125. A. Matsumoto, K. Sada, K. Tashiro, M. Miyata, T. Tsubouchi, T. Tanaka, T. Odani, S. Nagahama, T. Tanaka, K. Inoue, S. Saragai and S. Nakamoto, *Angew. Chem. Int. Ed.*, 2002, **41**, 2502-2505.
126. L. Dou, Y. Zheng, X. Shen, G. Wu, K. Fields, W.-C. Hsu, H. Zhou, Y. Yang and F. Wudl, *Science*, 2014, **343**, 272-277.
127. T. Hoang, J. W. Lauher and F. W. Fowler, *J. Am. Chem. Soc.*, 2002, **124**, 10656-10657.
128. T. Itoh, T. Suzuki, T. Uno, M. Kubo, N. Tohnai and M. Miyata, *Angew. Chem. Int. Ed.*, 2011, **50**, 2253-2256.
129. G. Wegner, *Z. Naturforsch.*, 1969, **24**, 824-832.
130. R. H. Baughman, *J. Appl. Phys.*, 2003, **43**, 4362-4370.

131. G. N. Patel, *Radiat. Phys. Chem.*, 1981, **18**, 913-925.
132. H. Tachibana, R. Kumai, N. Hosaka and Y. Tokura, *Chem. Mater.*, 2001, **13**, 155-158.
133. Y. L. Dory, M. Caron, V. O. Duguay, L. Chicoine-Ouellet, D. Fortin and P. Baillargeon, *Journal*, 2019, **9**.
134. H. Tabata, H. Tokoyama, H. Yamakado and T. Okuno, *J. Mater. Chem.*, 2012, **22**, 115-122.
135. T. Okuno, S. Ikeda, N. Kubo and D. J. Sandman, *Mol. Cryst. Liq. Cryst.*, 2006, **456**, 35-44.
136. S. Wang, Y. Li, H. Liu, J. Li, T. Li, Y. Wu, S. Okada and H. Nakanishi, *Org. Biomol. Chem.*, 2015, **13**, 5467-5474.
137. P. Tanphibal, K. Tashiro and S. Chirachanchai, *Macromol. Rapid Commun.*, 2016, **37**, 685-690.
138. Robert S. Jordan, Y. Wang, Ryan D. McCurdy, Michael T. Yeung, Kristofer L. Marsh, Saeed I. Khan, Richard B. Kaner and Y. Rubin, *Chem*, 2016, **1**, 78-90.
139. J. Deschamps, M. Balog, B. Boury, M. Ben Yahia, J.-S. Filhol, A. van der Lee, A. Al Choueiry, T. Barisien, L. Legrand, M. Schott and S. G. Dutremez, *Chem. Mater.*, 2010, **22**, 3961-3982.
140. H. Tabata, K. Kuwamoto and T. Okuno, *J. Mol. Struct.*, 2016, **1106**, 452-459.
141. R. Xu, W. B. Schweizer and H. Frauenrath, *J. Am. Chem. Soc.*, 2008, **130**, 11437-11445.
142. R. Xu, V. Gramlich and H. Frauenrath, *J. Am. Chem. Soc.*, 2006, **128**, 5541-5547.
143. J. J. Kane, T. Nguyen, J. Xiao, F. W. Fowler and J. W. Lauher, *Mol. Cryst. Liq. Cryst. Sci. Technol., Sect. A*, 2001, **356**, 449-458.
144. T. L. Nguyen, F. W. Fowler and J. W. Lauher, *J. Am. Chem. Soc.*, 2001, **123**, 11057-11064.
145. X. Ouyang, F. W. Fowler and J. W. Lauher, *J. Am. Chem. Soc.*, 2003, **125**, 12400-12401.
146. N. S. Goroff, S. M. Curtis, J. A. Webb, F. W. Fowler and J. W. Lauher, *Org. Lett.*, 2005, **7**, 1891-1893.
147. L. Luo, C. Wilhelm, A. Sun, C. P. Grey, J. W. Lauher and N. S. Goroff, *J. Am. Chem. Soc.*, 2008, **130**, 7702-7709.
148. Z. Li, F. W. Fowler and J. W. Lauher, *J. Am. Chem. Soc.*, 2009, **131**, 634-643.
149. A. Matsumoto, A. Matsumoto, T. Kunisue, A. Tanaka, N. Tohnai, K. Sada and M. Miyata, *Chem. Lett.*, 2003, **33**, 96-97.
150. A. Sun, J. W. Lauher and N. S. Goroff, *Science*, 2006, **312**, 1030-1034.
151. R. Khazeber and K. M. Sureshan, *Angew. Chem. Int. Ed.*, 2021, **60**, 24875-24881.
152. A. Ravi, A. Shijad and K. M. Sureshan, *Chem. Sci.*, 2021, **12**, 11652-11658.
153. R. Khazeber and K. M. Sureshan, *Proc. Natl. Acad. Sci.*, 2022, **119**, e2205320119.
154. V. Athiyarath, L. A. Mathew, Y. Zhao, R. Khazeber, U. Ramamurty and K. M. Sureshan, *Chem. Sci.*, 2023, **14**, 5132-5140.
155. C. Raju, G. R. Ramteke, K. V. J. Jose and K. M. Sureshan, *J. Am. Chem. Soc.*, 2023, **145**, 9607-9616.
156. S. Bhandary, A. Pathigoolla, M. C. Madhusudhanan and K. M. Sureshan, *Chem. - Eur. J.*, 2022, **28**, e202200820.
157. K. Hema and K. M. Sureshan, *Angew. Chem. Int. Ed.*, 2020, **59**, 8854-8859.
158. R. Mohanrao, K. Hema and K. M. Sureshan, *Nat. Commun.*, 2020, **11**, 865.
159. K. Wang, D. D. Qi, Y. L. Li, T. Y. Wang, H. B. Liu and J. Z. Jiang, *Coord. Chem. Rev.*, 2019, **378**, 188-206.
160. R.-B. Lin, Y. He, P. Li, H. Wang, W. Zhou and B. Chen, *Chem. Soc. Rev.*, 2019, **48**, 1362-1389.
161. H. Li, M. Eddaoudi, M. O'Keeffe and O. M. Yaghi, *Nature*, 1999, **402**, 276-279.
162. L. E. Kreno, K. Leong, O. K. Farha, M. Allendorf, R. P. Van Duyne and J. T. Hupp, *Chem. Rev.*, 2012, **112**, 1105-1125.
163. N. Stock and S. Biswas, *Chem. Rev.*, 2012, **112**, 933-969.
164. S. Horike, S. Shimomura and S. Kitagawa, *Nat. Chem.*, 2009, **1**, 695-704.
165. H. C. Zhou and S. Kitagawa, *Chem. Soc. Rev.*, 2014, **43**, 5415-5418.
166. M. Kondo, T. Yoshitomi, H. Matsuzaka, S. Kitagawa and K. Seki, *Angew. Chem. Int. Ed. Engl.*, 1997, **36**, 1725-1727.
167. C. Gropp, T. Ma, N. Hanikel and M. Yaghi Omar, *Science*, 2020, **370**, eabd6406.
168. M. Evans Austin, R. Parent Lucas, C. Flanders Nathan, P. Bisbey Ryan, E. Vitaku, S. Kirschner Matthew, D. Schaller Richard, X. Chen Lin, C. Gianneschi Nathan and R. Dichtel William, *Science*, 2018, **361**, 52-57.
169. A. Natraj, W. Ji, J. Xin, I. Castano, D. W. Burke, A. M. Evans, M. J. Strauss, M. Ateia, L. S. Hamachi, N. C. Gianneschi, Z. A. Alothman, J. Sun, K. Yusuf and W. R. Dichtel, *J. Am. Chem. Soc.*, 2022, **144**, 19813-19824.
170. C. Kang, K. Yang, Z. Zhang, A. K. Usadi, D. C. Calabro, L. S. Baugh, Y. Wang, J. Jiang, X. Zou, Z. Huang and D. Zhao, *Nat. Commun.*, 2022, **13**, 1370.
171. S. Patwardhan, A. A. Kocherzhenko, F. C. Grozema and L. D. A. Siebbeles, *J. Phys. Chem. C*, 2011, **115**, 11768-11772.
172. F. Auras, L. Ascherl, A. H. Hakimioun, J. T. Margraf, F. C. Hanusch, S. Reuter, D. Bessinger, M. Döblinger, C. Hettstedt, K. Karaghiosoff, S. Herbert, P. Knochel, T. Clark and T. Bein, *J. Am. Chem. Soc.*, 2016, **138**, 16703-16710.
173. J. Sakamoto, J. van Heijst, O. Lukin and A. D. Schlüter, *Angew. Chem. Int. Ed.*, 2009, **48**, 1030-1069.
174. R. Z. Lange, G. Hofer, T. Weber and A. D. Schlüter, *J. Am. Chem. Soc.*, 2017, **139**, 2053-2059.
175. G. M. J. Schmidt, 1971, **27**, 647-678.
176. F. Hu, W. Hao, D. Mücke, Q. Pan, Z. Li, H. Qi and Y. Zhao, *J. Am. Chem. Soc.*, 2021, **143**, 5636-5642.
177. X. Jiang, X. Cui, A. J. E. Duncan, L. Li, R. P. Hughes, R. J. Staples, E. V. Alexandrov, D. M. Proserpio, Y. Wu and C. Ke, *J. Am. Chem. Soc.*, 2019, **141**, 10915-10923.
178. Y. He, S. Xiang and B. Chen, *J. Am. Chem. Soc.*, 2011, **133**, 14570-14573.
179. R. Liang, J. Samanta, B. Shao, M. Zhang, R. J. Staples, A. D. Chen, M. Tang, Y. Wu, I. Aprahamian and C. Ke, *Angew. Chem. Int. Ed.*, 2021, **60**, 23176-23181.
180. J. Samanta, R. W. Dorn, W. Zhang, X. Jiang, M. Zhang, R. J. Staples, A. J. Rossini and C. Ke, *Chem*, 2022, **8**, 253-267.
181. R. Z. Lange, K. Synnatschke, H. Qi, N. Huber, G. Hofer, B. Liang, C. Huck, A. Pucci, U. Kaiser, C. Backes and A. D. Schlüter, *Angew. Chem. Int. Ed.*, 2020, **59**, 5683-5695.
182. J. Dong, L. Liu, C. Tan, Q. Xu, J. Zhang, Z. Qiao, D. Chu, Y. Liu, Q. Zhang, J. Jiang, Y. Han, A. P. Davis and Y. Cui, *Nature*, 2022, **602**, 606-611.
183. D. W. Burke, C. Sun, I. Castano, N. C. Flanders, A. M. Evans, E. Vitaku, D. C. McLeod, R. H. Lambeth, L. X. Chen, N. C. Gianneschi and W. R. Dichtel, *Angew. Chem. Int. Ed.*, 2020, **59**, 5165-5171.
184. X. D. Chen, Y. S. Li, L. Wang, Y. Xu, A. M. Nie, Q. Q. O. Li, F. Wu, W. W. Sun, X. Zhang, R. Vajtai, P. M. Ajayan, L. Chen and

Y. Wang, *Adv. Mater.*, 2019, **31**.
185. G. Das, B. P. Biswal, S. Kandambeth, V. Venkatesh, G. Kaur, M. Addicoat, T. Heine, S. Verma and R. Banerjee, *Chem. Sci.*, 2015, **6**, 3931-3939.
186. J. Q. Dong, X. Li, S. B. Peh, Y. D. Yuan, Y. X. Wang, D. X. Ji, S. J. Peng, G. L. Liu, S. M. Ying, D. Q. Yuan, J. W. Jiang, S. Ramakrishna and D. Zhao, *Chem. Mater.*, 2019, **31**, 146-160.
187. D. Rodriguez-San-Miguel, C. Montoro and F. Zamora, *Chem. Soc. Rev.*, 2020, **49**, 2291-2302.
188. S. Wang, Q. Y. Wang, P. P. Shao, Y. Z. Han, X. Gao, L. Ma, S. Yuan, X. J. Ma, J. W. Zhou, X. Feng and B. Wang, *J. Am. Chem. Soc.*, 2017, **139**, 4258-4261.
189. V. Müller, F. Shao, M. Baljozovic, M. Moradi, Y. Zhang, T. Jung, W. B. Thompson, B. T. King, R. Zenobi and A. D. Schlüter, *Angew. Chem. Int. Ed.*, 2017, **56**, 15262-15266.
190. W. Dai, F. Shao, J. Szczerbiński, R. McCaffrey, R. Zenobi, Y. Jin, A. D. Schlüter and W. Zhang, *Angew. Chem. Int. Ed.*, 2016, **55**, 213-217.
191. V. Müller, A. Hinaut, M. Moradi, M. Baljozovic, T. A. Jung, P. Shahgaldian, H. Möhwald, G. Hofer, M. Kröger, B. T. King, E. Meyer, T. Glatzel and A. D. Schlüter, *Angew. Chem. Int. Ed.*, 2018, **57**, 10584-10588.
192. K. Liu, H. Qi, R. Dong, R. Shivhare, M. Addicoat, T. Zhang, H. Sahabudeen, T. Heine, S. Mannsfeld, U. Kaiser, Z. Zheng and X. Feng, *Nat. Chem.*, 2019, **11**, 994-1000.
193. R. H. Dong, T. Zhang and X. L. Feng, *Chem. Rev.*, 2018, **118**, 6189-6235.
194. T. Zhang, H. Qi, Z. Liao, Y. D. Horev, L. A. Panes-Ruiz, P. S. Petkov, Z. Zhang, R. Shivhare, P. Zhang, K. Liu, V. Bezugly, S. Liu, Z. Zheng, S. Mannsfeld, T. Heine, G. Cuniberti, H. Haick, E. Zschech, U. Kaiser, R. Dong and X. Feng, *Nat. Commun.*, 2019, **10**, 4225.
195. H. Sahabudeen, H. Qi, M. Ballabio, M. Položij, S. Olthof, R. Shivhare, Y. Jing, S. Park, K. Liu, T. Zhang, J. Ma, B. Rellinghaus, S. Mannsfeld, T. Heine, M. Bonn, E. Cánovas, Z. Zheng, U. Kaiser, R. Dong and X. Feng, *Angew. Chem. Int. Ed.*, 2020, **59**, 6028-6036.
196. Z. Zhang, C. Wu, Q. Pan, F. Shao, Q. Sun, S. Chen, Z. Li and Y. Zhao, *Chem. Commun.*, 2020, **56**, 3210-3213.
197. Q. Sun, Q. Pan, Y. Ban, H. Liu, C. Fan, L. Sun and Y. Zhao, *Chem. - Eur. J.*, 2021, **27**, 3661-3664.
198. H. Sahabudeen, H. Y. Qi, B. A. Glatz, D. Tranca, R. H. Dong, Y. Hou, T. Zhang, C. Kuttner, T. Lehnert, G. Seifert, U. Kaiser, A. Fery, Z. K. Zheng and X. L. Feng, *Nat. Commun.*, 2016, **7**.
199. F. L. Tan, S. Han, D. L. Peng, H. L. Wang, J. Yang, P. Zhao, X. J. Ye, X. Dong, Y. Y. Zheng, N. Zheng, L. Gong, C. L. Liang, N. Frese, A. Golzhauser, H. Y. Qi, S. S. Chen, W. Liu and Z. K. Zheng, *J. Am. Chem. Soc.*, 2021, **143**, 3927-3933.
200. R. Matsuoka, R. Sakamoto, K. Hoshiko, S. Sasaki, H. Masunaga, K. Nagashio and H. Nishihara, *J. Am. Chem. Soc.*, 2017, **139**, 3145-3152.
201. K. Dey, M. Pal, K. C. Rout, H. S. Kunjattu, A. Das, R. Mukherjee, U. K. Kharul and R. Banerjee, *J. Am. Chem. Soc.*, 2017, **139**, 13083-13091.
202. M. Matsumoto, L. Valentino, G. M. Stiehl, H. B. Balch, A. R. Corcos, F. Wang, D. C. Ralph, B. J. Marinas and W. R. Dichtel, *Chem*, 2018, **4**, 308-317.
203. D. Zhou, X. Y. Tan, H. M. Wu, L. H. Tian and M. Li, *Angew. Chem. Int. Ed.*, 2019, **58**, 1376-1381.
204. X. L. Feng and A. D. Schluter, *Angew. Chem. Int. Ed.*, 2018, **57**, 13748-13763.
205. Y. Jin, Y. Hu, M. Ortiz, S. Huang, Y. Ge and W. Zhang, *Chem. Soc. Rev.*, 2020, **49**, 4637-4666.
206. X. Chen, S. Yamanaka, K. Sako, Y. Inoue and M. Yasukawa, *Chem. Phys. Lett.*, 2002, **356**, 291-297.
207. M. Núñez-Regueiro, L. Marques, J. L. Hodeau, O. Béthoux and M. Perroux, *Phys. Rev. Lett.*, 1995, **74**, 278-281.
208. S. Yamanaka, A. Kubo, K. Inumaru, K. Komaguchi, N. S. Kini, T. Inoue and T. Irifune, *Phys. Rev. Lett.*, 2006, **96**, 076602.
209. X. Chen and S. Yamanaka, *Chem. Phys. Lett.*, 2002, **360**, 501-508.
210. V. D. Blank, S. G. Buga, G. A. Dubitsky, N. R. Serebryanaya, M. Y. Popov and B. Sundqvist, *Carbon*, 1998, **36**, 319-343.
211. Y. Iwasa, T. Arima, R. M. Fleming, T. Siegrist, O. Zhou, R. C. Haddon, L. J. Rothberg, K. B. Lyons, H. L. Carter, A. F. Hebard, R. Tycko, G. Dabbagh, J. J. Krajewski, G. A. Thomas and T. Yagi, *Science*, 1994, **264**, 1570-1572.
212. S. Margadonna, D. Pontiroli, M. Belli, T. Shiroka, M. Riccò and M. Brunelli, *J. Am. Chem. Soc.*, 2004, **126**, 15032-15033.
213. P. W. Stephens, G. Bortel, G. Faigel, M. Tegze, A. Jánossy, S. Pekker, G. Oszlanyi and L. ForrÓ, *Nature*, 1994, **370**, 636-639.
214. A. F. Hebard, M. J. Rosseinsky, R. C. Haddon, D. W. Murphy, S. H. Glarum, T. T. M. Palstra, A. P. Ramirez and A. R. Kortan, *Nature*, 1991, **350**, 600-601.
215. M. J. Rosseinsky, A. P. Ramirez, S. H. Glarum, D. W. Murphy, R. C. Haddon, A. F. Hebard, T. T. M. Palstra, A. R. Kortan, S. M. Zahurak and A. V. Makhija, *Phys. Rev. Lett.*, 1991, **66**, 2830-2832.
216. S. Margadonna and K. Prassides, *J. Solid State Chem.*, 2002, **168**, 639-652.
217. L. Forró and L. Mihály, *Rep. Prog. Phys.*, 2001, **64**, 649-699.
218. R. P. Gupta and M. Gupta, *Phys. C*, 1994, **219**, 21-25.
219. D. W. Murphy, M. J. Rosseinsky, R. M. Fleming, R. Tycko, A. P. Ramirez, R. C. Haddon, T. Siegrist, G. Dabbagh, J. C. Tully and R. E. Walstedt, *J. Phys. Chem. Solids*, 1992, **53**, 1321-1332.
220. M. Tanaka and S. Yamanaka, *Cryst. Growth Des.*, 2018, **18**, 3877-3882.
221. L. Hou, X. Cui, B. Guan, S. Wang, R. Li, Y. Liu, D. Zhu and J. Zheng, *Nature*, 2022, **606**, 507-510.
222. L. Liang, Y. Qiu, W. D. Wang, J. Han, Y. Luo, W. Yu, G.-L. Yin, Z.-P. Wang, L. Zhang, J. Ni, J. Niu, J. Sun, T. Ma and W. Wang, *Angew. Chem. Int. Ed.*, 2020, **59**, 17991-17995.
223. C. Gao, J. Li, S. Yin, J. Sun and C. Wang, *J. Am. Chem. Soc.*, 2020, **142**, 3718-3723.
224. X. Liu, J. Li, B. Gui, G. Lin, Q. Fu, S. Yin, X. Liu, J. Sun and C. Wang, *J. Am. Chem. Soc.*, 2021, **143**, 2123-2129.
225. Y. Xie, J. Li, C. Lin, B. Gui, C. Ji, D. Yuan, J. Sun and C. Wang, *J. Am. Chem. Soc.*, 2021, **143**, 7279-7284.
226. C. Gao, J. Li, S. Yin, J. Sun and C. Wang, *Nat. Commun.*, 2020, **11**, 4919.
227. Y. Liu, P. Chen, Y. Wang, J. Suo, J. Ding, L. Zhu, V. Valtchev, Y. Yan, S. Qiu, J. Sun and Q. Fang, *Angew. Chem. Int. Ed.*, 2022, **61**, e202203584.
228. F. Jin, E. Lin, T. Wang, S. Geng, L. Hao, Q. Zhu, Z. Wang, Y. Chen, P. Cheng and Z. Zhang, *J. Am. Chem. Soc.*, 2022, **144**, 23081-23088.
229. Z. Zhou, L. Zhang, Y. Yang, I. J. Vitorica-Yrezabal, H. Wang, F. Tan, L. Gong, Y. Li, P. Chen, X. Dong, Z. Liang, J. Yang, C. Wang, Y. Hong, Y. Qiu, A. Gölzhäuser, X. Chen, H. Qi, S. Yang, W. Liu, J. Sun and Z. Zheng, *Nat. Chem.*, 2023, **15**, 841-847.
230. Y. Liu, Y. Ma, Y. Zhao, X. Sun, F. Gándara, H. Furukawa, Z. Liu, H. Zhu, C. Zhu, K. Suenaga, P. Oleynikov, S. Alshammari

Ahmad, X. Zhang, O. Terasaki and M. Yaghi Omar, *Science*, 2016, **351**, 365-369.

231. Y. Zhao, L. Guo, F. Gándara, Y. Ma, Z. Liu, C. Zhu, H. Lyu, C. A. Trickett, E. A. Kapustin, O. Terasaki and O. M. Yaghi, *J. Am. Chem. Soc.*, 2017, **139**, 13166-13172.
232. Y. Liu, Y. Ma, J. Yang, C. S. Diercks, N. Tamura, F. Jin and O. M. Yaghi, *J. Am. Chem. Soc.*, 2018, **140**, 16015-16019.
233. Y. Liu, C. S. Diercks, Y. Ma, H. Lyu, C. Zhu, S. A. Alshmimri, S. Alshihri and O. M. Yaghi, *J. Am. Chem. Soc.*, 2019, **141**, 677-683.
234. C. Sun, J. J. Oppenheim, G. Skorupskii, L. Yang and M. Dincă, *Chem*, 2022, **8**, 3215-3224.